The Astrophysical Journal, 752:14 (19pp), 2012 June 10 doi:10.1088/0004-637X/752/1/14

STRONG TIDAL DISSIPATION IN SATURN AND CONSTRAINTS ON ENCELADUS' THERMAL STATE FROM ASTROMETRY

Valéry Lainey[1], Özgür Karatekin[2], Josselin Desmars[1,3], Sébastien Charnoz[4], Jean-Eudes Arlot[1], Nicolai Emelyanov[1,5], Christophe Le Poncin-Lafitte[6], Stéphane Mathis[4], Françoise Remus[1,4,7], Gabriel Tobie[8], and Jean-Paul Zahn[7]

[1] IMCCE-Observatoire de Paris, UMR 8028 du CNRS, UPMC, 77 Av. Denfert-Rochereau, 75014 Paris, France; lainey@imcce.fr
[2] Royal Observatory of Belgium, Avenue Circulaire 3, 1180 Uccle, Bruxelles, Belgium
[3] Shanghai Astronomical Observatory, Chinese Academy of Sciences, 80 Nandan Road, 200030 Shanghai, China
[4] Laboratoire AIM, CEA/DSM-CNRS-Université Paris Diderot, IRFU/SAp Centre de Saclay, 91191 Gif-sur-Yvette, France
[5] Sternberg Astronomical Institute, 13 Universitetskij Prospect, 119992 Moscow, Russia
[6] SyRTE-Observatoire de Paris, UMR 8630 du CNRS, 77 Av. Denfert-Rochereau, 75014 Paris, France
[7] LUTH-Observatoire de Paris, UMR 8102 du CNRS, 5 place Jules Janssen, 92195 Meudon Cedex, France
[8] Laboratoire de Planétologie et Géodynamique de Nantes, Université de Nantes, CNRS, UMR 6112, 2 rue de la Houssinière, 44322 Nantes Cedex 3, France
Received 2011 September 4; accepted 2012 March 23; published 2012 May 22

ABSTRACT

Tidal interactions between Saturn and its satellites play a crucial role in both the orbital migration of the satellites and the heating of their interiors. Therefore, constraining the tidal dissipation of Saturn (here the ratio k_2/Q) opens the door to the past evolution of the whole system. If Saturn's tidal ratio can be determined at different frequencies, it may also be possible to constrain the giant planet's interior structure, which is still uncertain. Here, we try to determine Saturn's tidal ratio through its current effect on the orbits of the main moons, using astrometric data spanning more than a century. We find an intense tidal dissipation ($k_2/Q = (2.3 \pm 0.7) \times 10^{-4}$), which is about 10 times higher than the usual value estimated from theoretical arguments. As a consequence, eccentricity equilibrium for Enceladus can now account for the huge heat emitted from Enceladus' south pole. Moreover, the measured k_2/Q is found to be poorly sensitive to the tidal frequency, on the short frequency interval considered. This suggests that Saturn's dissipation may not be controlled by turbulent friction in the fluid envelope as commonly believed. If correct, the large tidal expansion of the moon orbits due to this strong Saturnian dissipation would be inconsistent with the moon formations 4.5 Byr ago above the synchronous orbit in the Saturnian subnebulae. But it would be compatible with a new model of satellite formation in which the Saturnian satellites formed possibly over a longer timescale at the outer edge of the main rings. In an attempt to take into account possible significant torques exerted by the rings on Mimas, we fitted a constant rate da/dt on Mimas' semi-major axis as well. We obtained an unexpected large acceleration related to a negative value of $da/dt = -(15.7 \pm 4.4) \times 10^{-15}$ AU day^{-1}. Such acceleration is about an order of magnitude larger than the tidal deceleration rates observed for the other moons. If not coming from an astrometric artifact associated with the proximity of Saturn's halo, such orbital decay may have significant implications on the Saturn's rings.

Key words: astrometry – celestial mechanics – ephemerides – Planets and satellites: dynamical evolution and stability – Planets and satellites: interiors

Online-only material: color figures

1. INTRODUCTION

Starting with Huygens' observation of Titan in 1655, a little less than two centuries were needed to discover the so-called main moons of Saturn (defined by increasing distance to the primary, Mimas, Enceladus, Tethys, Dione, Rhea, Titan, Hyperion, and Iapetus). In common with the Galilean moons, astrometry of the Saturn satellites (consisting of measuring the moon positions in the sky) started in the middle of the 17th century, with the observations of eclipses by the primary. One has to wait until the end of the 19th century and the manufacturing of photographic plates, as well as large micrometer and heliometer instruments, for the gathering of reasonably accurate observations (Desmars et al. 2009b). Although previously used to probe the gravity fields of the system, astrometry has been replaced advantageously by radio-science data, since the spacecraft era. Nevertheless, the large time span covered by astrometric observations and number of observation sets available can still compensate for any possible lack of precision when one focuses on long-term dynamical effects, as, for example, in the case of Mars (Lainey et al. 2007) and Jupiter (Lainey et al. 2009).

In Section 2, we present the observation set used in this study. Section 3 details the numerical model of the Saturnian satellite orbits that has been used to determine Saturn's tidal dissipation. In Sections 4 and 5, we present the fit of the orbit model to astrometric observations and demonstrate its robustness. The last section discusses possible interior models of Saturn and Enceladus in the light of our results.

2. THE OBSERVATION SET

To determine long-term effects in the mean motions of the satellites accurately, a set of astrometric observations covering a long time span is necessary. In this context, an extensive catalog of astrometric observations has been compiled. This catalog provides about 19,617 observations (counting one date as one observation even for several satellites observed simultaneously) and covers the period from 1886 to 2009. All observations are available in the NSDB natural satellites astrometric database (Arlot & Emelyanov 2009).

The main source of the catalog is COSS08 (Desmars et al. 2009b), yielding about 130,000 data (counting one coordinate of one satellite as one datum) from 1874 to 2007. For our set of data, only the "accurate" observations have been selected. To define "accurate" observations, we have first excluded those with a residual larger than 2 arcsec and then computed the rms of the residuals for all the observations corresponding to each bibliographic reference. Finally, for the purposes of the present paper, if the rms was larger than 0.3 arcsec for observations before 1950 and 0.25 arcsec for observations after 1950, the entire set issued from that particular bibliographic reference has been excluded. As a consequence, about 93% of COSS08 observations have been selected starting from 1886 until 2007.

Since 2007, other observations have become available. The USNO Flagstaff transit circle data, already included in COSS08, have been updated until 2009. Observations from Peng et al. (2008) have also been added. Moreover, the highly accurate astrometric observations provided by the observation of the mutual phenomena of Saturnian satellites during 1995 and 2009 have been added.

Finally, the extensive catalog contains about 19,000 observations made from 1886 to 2009.

Direct astrometric observations can be performed in several different ways: transit observations, photographic plates, and CCD imaging. They are reduced from the known position of reference stars visible in the field of view during the observation. Because of their small field of view, the CCD frames and some long focus photographic plates do not often allow the use of reference stars. To deal with such data, the authors generally use the position of specific well-known satellites (usually Titan, Rhea, Dione, and Tethys because of their accurate ephemerides) computed with a specific theory as a reference in order to deduce the astrometric positions of the other satellites. A drawback of this is that these observations may be biased by any limiting assumptions in the adopted theory. To deal with this problem, we preferred to consider only relative separation and position angle between the satellites using pixel positions. This method provides astrometric observations that do not depend on the theory. It has been applied for CCD observations when stars were not used in the astrometric reduction. The influence of such a bias is tested in Section 5.3.

Photometric observations of mutual occultations and eclipses of the Saturnian satellites provide very accurate astrometric relative positions of the satellites. These observations are possible during the Saturnian equinox, since the Sun and the Earth are then in the equatorial plane of Saturn, which is also the common orbital plane of the satellites. Campaigns of observations of such mutual occultations and eclipses were made in 1995 and 2009. We undertook the processing of the complete database of these photometric observations published by Thuillot et al. (2001). An accurate photometric model of mutual events using the scattering properties of the satellite surfaces (Buratti 1984) issued from *Voyager* data was used. A large analysis of the properties of Saturnian icy satellites is done in Pitman et al. (2010) using the observations of these bodies provided by the *Cassini* probe. Phase curves are given in the V and R bands for solar phase angles in the vaste range up to 180° (but only for Rhea and Dione). Unfortunately, because of this wide range of phase angles, we could not rely on Pitman et al. (2010) for the satellite albedo in the range of 1°–6° and therefore did not use their data.

In order to extract astrometric positions from photometric data, we developed an original method (Emelyanov & Gilbert 2006). We have processed the 46 light curves obtained during the international campaign of photometric observations of the Saturnian satellites in 1995 and the 17 light curves obtained during the international campaign in 2009. From these photometric observations 46 topocentric or heliocentric angular differences in right ascension and declination for satellite pairs on the time interval from 1995 December 16 to 1996 February 6 and 17 topocentric or heliocentric angular differences on the time interval from 2008 December 19 to 2009 July 7 were obtained. The errors due to random errors of photometry are from 1 to 15 mas in right ascension and declination and characterize the internal accuracy of the astrometric results. Nevertheless, due to the rather small number of observed events compared to other observation sets, the contribution of mutual events has turned out to be modest. This contrasts with the Jovian case (Lainey et al. 2009).

3. THE DYNAMICAL MODEL

The NOE (Numerical Orbit and Ephemerides) numerical code (Lainey et al. 2007, 2009; Lainey 2008) has been used to model the orbital motion of the Saturnian satellites. It is a gravitational N-body code that incorporates highly sensitive modeling and can generate partial derivatives needed to fit initial positions, velocities, and other parameters (like the ratio k_2/Q) to the observational data. The code includes (1) gravitational interaction up to degree two in the spherical harmonic expansion of the gravitational potential for the satellites and up to degree six for Saturn with the numerical values from Jacobson et al. (2006), (2) perturbations due to the Sun and Jupiter using DE406 ephemerides (with the inner planets and the Moon included by incorporating their masses in the solar value), (3) Saturnian precession from Jacobson (2007), and (4) tidal effects introduced by means of the Love number k_2 and the quality factor Q in the combination k_2/Q for Saturn and Enceladus. The orbital effects due to the dissipation inside Saturnian satellites other than Enceladus are neglected, since they are expected to be much less dissipative, less eccentric, or much farther away from Saturn. Nevertheless, the tidal bulges raised by each moon on Saturn are taken into account.

The dynamical equations are numerically integrated in a Saturn-centric frame with inertial axes (conveniently the Earth mean equator J2000). The equation of motion for a satellite P_i can be expressed in a general form as

$$\begin{aligned}\ddot{\boldsymbol{r}}_i = &-G(m_0+m_i)\left(\frac{\boldsymbol{r}_i}{r_i^3} - \nabla_i U_{\bar{i}\hat{0}} + \nabla_0 U_{\bar{0}\hat{i}}\right) + \sum_{j=1, j\neq i}^{N} G m_j \\ &\times \left(\frac{\boldsymbol{r}_j - \boldsymbol{r}_i}{r_{ij}^3} - \frac{\boldsymbol{r}_j}{r_j^3} - \nabla_j U_{\bar{j}\hat{i}} + \nabla_i U_{\bar{i}\hat{j}} + \nabla_j U_{\bar{j}\hat{0}} - \nabla_0 U_{\bar{0}\hat{j}}\right) \\ &+ \frac{(m_0+m_i)}{m_i m_0}\left(\boldsymbol{F}^T_{\bar{i}\hat{0}} - \boldsymbol{F}^T_{\bar{0}\hat{i}}\right) - \frac{1}{m_0}\sum_{j=1, j\neq i}^{N}\left(\boldsymbol{F}^T_{\bar{j}\hat{0}} - \boldsymbol{F}^T_{\bar{0}\hat{j}}\right).\end{aligned} \tag{1}$$

Here, $\boldsymbol{r}_i$ and $\boldsymbol{r}_j$ are the position vectors of the satellite P_i and a body P_j (another satellite, the Sun, or Jupiter) with mass m_j, subscript 0 denotes Saturn, $U_{\hat{k}\hat{l}}$ is the oblateness gravity field of body P_l at the position of body P_k, and $\boldsymbol{F}^T_{\bar{l}\hat{k}}$ is the force received by P_l from the tides it raises on P_k. This force is equal to (Lainey

Table 1
Statistics of the Astrometric Residuals Computed from Our Model (Enceladus Tidal Equilibrium Solution) in Arcsecond

Observation subset	$\nu_\alpha \cos(\delta)$	$\sigma_{\alpha\cos(\delta)}$	ν_δ	σ_δ	N_α, N_δ
All observations					
S1	−0.0057	0.0952	−0.0108	0.0725	371, 371
S2	0.0019	0.1040	0.0028	0.1101	822, 822
S3	−0.0199	0.1267	0.0122	0.1067	1972, 1972
S4	0.0020	0.1066	0.0113	0.1067	2271, 2271
S5	0.0047	0.0899	−0.0023	0.0863	2977, 2977
S6	0.0121	0.1060	−0.0171	0.1070	3271, 3271
S7	0.1098	0.2984	0.0036	0.2166	973, 973
S8	0.0140	0.1143	−0.0052	0.1155	2008, 2008
Alden & O'Connel (1928)					
S2	0.0193	0.0890	0.0394	0.0816	40, 40
S3	0.0267	0.0653	0.0066	0.0569	65, 65
S4	0.0218	0.0493	0.0119	0.0467	64, 64
S5	0.0007	0.0563	0.0204	0.0528	64, 64
S6	−0.0442	0.0681	−0.0076	0.0566	64, 64
S8	−0.0190	0.1538	−0.0609	0.1337	59, 59
Alden (1929)					
S2	0.0258	0.0819	0.0228	0.0794	34, 34
S3	0.0031	0.0420	0.0127	0.0526	38, 38
S4	0.0097	0.0349	0.0359	0.0352	34, 34
S5	−0.0233	0.0520	0.0306	0.0364	36, 36
S6	−0.0267	0.0516	−0.0132	0.0508	36, 36
S8	0.0135	0.0727	−0.0887	0.1006	35, 35
Sinclair (1974, 1977) 13s					
S3	0.0279	0.1090	−0.0107	0.1446	20, 20
S4	0.0317	0.1551	0.0350	0.1528	25, 25
S5	0.0040	0.1099	−0.0330	0.0952	25, 25
S6	−0.1788	0.1799	0.0310	0.0819	25, 25
S8	0.1258	0.1603	−0.0254	0.1186	24, 24
Sinclair (1974, 1977) 26s					
S3	0.0005	0.1069	0.0124	0.1011	40, 40
S4	0.0044	0.0592	0.0098	0.0626	46, 46
S5	0.0054	0.0698	−0.0122	0.0805	48, 48
S6	−0.0002	0.0823	−0.0079	0.0555	48, 48
S8	−0.0099	0.0563	0.0004	0.0821	48, 48
Abbot et al. (1975) PDS					
S1	−0.1707	0.0000	−0.0859	0.0000	1, 1
S2	−0.0472	0.0901	0.1828	0.1098	4, 4
S3	−0.0068	0.1408	0.1060	0.1260	10, 10
S4	−0.0476	0.1199	0.0084	0.0622	10, 10
S5	0.0344	0.0347	0.0109	0.0371	10, 10
S6	−0.0693	0.0702	−0.0587	0.0241	11, 11
S7	−0.2607	0.1166	0.3553	0.0757	6, 6
S8	0.0138	0.0739	0.0475	0.0274	10, 10
Abbot et al. (1975) Mann					
S1	0.0692	0.0000	−0.1231	0.0000	1, 1
S2	−0.1171	0.0981	0.3500	0.2047	5, 5
S3	0.0028	0.0888	0.0298	0.1325	11, 11
S4	−0.0321	0.1280	0.0584	0.1849	11, 11
S5	0.0393	0.0448	0.0136	0.0761	11, 11
S6	−0.0960	0.1324	−0.0234	0.0385	11, 11
S7	−0.2767	0.0599	0.4871	0.0485	6, 6
S8	0.0325	0.0941	0.0465	0.0559	11, 11
Voronenko et al. (1991)					
S3	0.0172	0.2064	−0.0056	0.1350	85, 85
S4	−0.0324	0.1675	0.0066	0.1712	96, 96
S5	−0.0034	0.1455	0.0214	0.0976	143, 143
S6	0.0179	0.1319	−0.0196	0.1084	153, 153
S8	0.0154	0.1679	−0.0263	0.1085	19, 19
D. Pascu (1982, private communication)					
S1	−0.0105	0.1620	−0.0393	0.1155	56, 56
S2	0.0041	0.0953	−0.0228	0.1208	107, 107

Table 1
(Continued)

Observation subset	$v_\alpha \cos(\delta)$	$\sigma_{\alpha\cos(\delta)}$	v_δ	σ_δ	N_α, N_δ
S3	0.0148	0.0644	−0.0104	0.0775	138, 138
S4	−0.0001	0.0505	−0.0064	0.0608	165, 165
S5	0.0115	0.0502	−0.0041	0.0602	209, 209
S6	−0.0010	0.0529	0.0153	0.0644	228, 228
S7	0.0761	0.2466	−0.0564	0.1824	11, 11
S8	−0.0191	0.0886	0.0211	0.1071	213, 213
Tolbin (1991a)					
S1	−0.0297	0.1602	−0.0414	0.1813	21, 21
S2	0.0059	0.0884	0.0090	0.1327	57, 57
S3	0.0004	0.0697	−0.0180	0.0834	75, 75
S4	0.0127	0.0551	−0.0073	0.0856	81, 81
S5	0.0016	0.0526	0.0047	0.0684	88, 88
S6	0.0033	0.0758	−0.0022	0.0968	89, 89
S8	−0.0194	0.1521	0.0336	0.1261	62, 62
Tolbin (1991b)					
S1	0.0292	0.1520	0.0194	0.1375	7, 7
S2	−0.0120	0.1237	0.0266	0.1293	50, 50
S3	0.0003	0.0596	−0.0037	0.0767	89, 89
S4	0.0121	0.0587	−0.0006	0.0706	96, 96
S5	0.0012	0.0617	−0.0041	0.0817	102, 102
S6	0.0067	0.0674	−0.0354	0.1222	107, 107
S8	−0.0189	0.0740	0.0309	0.1920	80, 80
Seitzer & Ianna (1980)					
S3	−0.0879	0.0096	0.0504	0.0297	3, 3
S4	−0.0332	0.0198	−0.0141	0.0109	3, 3
S5	0.0654	0.0629	−0.1057	0.0739	10, 10
S6	0.0454	0.0849	−0.0381	0.0600	17, 17
S8	−0.0515	0.1236	0.0060	0.1843	24, 24
Taylor & Sinclair (1985)					
S2	0.0604	0.1549	0.0443	0.0569	10, 10
S3	0.0710	0.1993	0.0589	0.0852	20, 20
S4	−0.0485	0.1979	0.0097	0.1309	35, 35
S5	0.0250	0.1227	−0.0005	0.1180	38, 38
S6	−0.0078	0.0973	−0.0696	0.1138	45, 45
S7	0.2277	0.5327	0.0817	0.5884	38, 38
S8	−0.0152	0.1239	0.0405	0.1432	45, 45
Seitzer et al. (1979)					
S1	−0.1067	0.1613	−0.0564	0.0106	2, 2
S3	0.0055	0.0678	−0.0073	0.0849	49, 49
S4	0.0539	0.2094	−0.1229	0.1929	41, 41
S5	0.0082	0.0652	−0.0387	0.0756	49, 49
S6	0.0829	0.1042	−0.0467	0.1039	50, 50
S7	−0.3379	0.1333	0.0453	0.1124	4, 4
S8	−0.0430	0.0971	0.1102	0.1839	60, 60
Dourneau et al. (1986)					
S1	0.0686	0.2278	−0.0274	0.1042	11, 11
S2	0.0146	0.1244	−0.0151	0.0593	39, 39
S3	0.0249	0.0786	−0.0285	0.0488	39, 39
S4	−0.0259	0.0691	−0.0260	0.0570	56, 56
S5	0.0045	0.0644	−0.0097	0.0478	76, 76
S6	0.0101	0.0684	0.0549	0.0426	82, 82
S7	0.7665	0.1130	0.0276	0.0832	95, 95
S8	−0.0126	0.1165	−0.0019	0.0698	95, 95
Veillet & Dourneau (1992) 3.6					
S3	0.0037	0.0858	−0.0083	0.1542	20, 20
S4	0.0630	0.1749	−0.0281	0.1058	25, 25
S5	0.0651	0.0404	−0.0392	0.0561	14, 14
S6	−0.0164	0.1288	−0.1052	0.0773	17, 17
S7	0.1865	0.3238	−0.0286	0.0985	25, 25
S8	−0.0763	0.1239	0.1069	0.0649	30, 30
Veillet & Dourneau (1992) 1.5					
S1	−0.1346	0.1196	−0.0500	0.0749	10, 10
S2	−0.0014	0.1013	−0.0223	0.0880	57, 57

Table 1
(Continued)

Observation subset	$v_\alpha \cos(\delta)$	$\sigma_{\alpha\cos(\delta)}$	v_δ	σ_δ	N_α, N_δ
S3	−0.0083	0.1103	0.0007	0.0807	78, 78
S4	0.0112	0.0689	−0.0032	0.0674	155, 155
S5	0.0028	0.0542	−0.0019	0.0495	195, 195
S6	−0.0015	0.0671	0.0167	0.0479	197, 197
S7	0.0006	0.1234	0.0118	0.0916	197, 197
S8	0.0004	0.0874	−0.0037	0.0976	196, 196
Kiseleva et al. (1996)					
S2	−0.0420	0.0940	0.0219	0.1574	10, 10
S3	−0.0168	0.0868	0.0413	0.1150	11, 11
S4	−0.0057	0.0507	−0.0251	0.0566	25, 25
S5	−0.0211	0.0623	−0.0188	0.0792	25, 25
S6	−0.0036	0.0592	−0.0081	0.0834	32, 32
S8	0.0662	0.0902	0.0325	0.1311	21, 21
Vass (1997)					
S2	0.0025	0.1647	−0.0132	0.1532	151, 151
S3	−0.0704	0.1494	0.0319	0.1246	654, 654
S4	−0.0039	0.1388	0.0480	0.1269	600, 600
S5	0.0061	0.1237	−0.0059	0.1135	948, 948
S6	0.0083	0.1163	−0.0203	0.1193	1287, 1287
S7	−0.0477	0.1564	0.0478	0.2366	94, 94
S8	0.1306	0.1505	−0.0654	0.1037	243, 243
Kiseleva & Kalinitchenko (2000)					
S1	−0.1235	0.0434	0.0449	0.0373	3, 3
S2	−0.0387	0.0923	0.0023	0.0716	10, 10
S3	−0.0165	0.0654	0.0182	0.0748	22, 22
S4	0.0239	0.0527	−0.0236	0.0686	23, 23
S5	0.0039	0.0532	0.0138	0.0594	27, 27
S6	0.0100	0.0564	0.0069	0.0768	27, 27
S8	0.0139	0.1079	−0.0410	0.1718	14, 14
Kiseleva & Kalinitchenko (1998)					
S2	−0.0768	0.1335	0.2952	0.1175	3, 3
S3	−0.0178	0.0415	−0.0342	0.1405	7, 7
S4	0.0509	0.0714	−0.0259	0.1535	4, 4
S5	−0.0124	0.0384	−0.0070	0.0762	10, 10
S6	0.0386	0.0718	−0.0818	0.2194	12, 12
S8	0.0117	0.0000	−0.0871	0.0000	1, 1
French et al. (2006) HST-WF4					
S1	−0.0002	0.0111	−0.0093	0.0104	39, 39
S2	0.0025	0.0132	0.0005	0.0157	53, 53
S3	0.0039	0.0167	0.0057	0.0160	63, 63
S4	0.0027	0.0196	0.0054	0.0269	33, 33
S5	−0.0011	0.0152	0.0014	0.0199	39, 39
S6	−0.0273	0.0401	−0.0107	0.0328	23, 23
S7	0.0856	0.0074	0.0009	0.0040	4, 4
French et al. (2006) HST-PC					
S1	0.0022	0.0076	0.0004	0.0098	154, 154
S2	−0.0027	0.0056	−0.0001	0.0087	82, 82
S3	0.0056	0.0124	0.0031	0.0077	24, 24
S4	−0.0112	0.0024	−0.0122	0.0013	5, 5
S5	0.0083	0.0060	0.0049	0.0081	10, 10
French et al. (2006) HST-WF3					
S1	0.0037	0.0079	−0.0030	0.0173	25, 25
S2	−0.0034	0.0117	−0.0026	0.0130	51, 51
S3	0.0011	0.0086	0.0007	0.0142	55, 55
S4	0.0024	0.0187	−0.0087	0.0193	99, 99
S5	−0.0022	0.0166	0.0012	0.0291	70, 70
S7	−0.0119	0.0095	−0.0148	0.0301	13, 13
French et al. (2006) HST-WF2					
S1	0.0022	0.0119	0.0034	0.0135	34, 34
S2	−0.0020	0.0160	0.0119	0.0111	35, 35
S3	0.0042	0.0111	−0.0073	0.0206	33, 33
S4	0.0089	0.0199	0.0074	0.0281	87, 87

Table 1
(Continued)

Observation subset	$\nu_\alpha \cos(\delta)$	$\sigma_{\alpha\cos(\delta)}$	ν_δ	σ_δ	N_α, N_δ
S5	−0.0127	0.0140	−0.0105	0.0223	35, 35
S7	0.0030	0.0509	0.0234	0.0189	30, 30
USNO Flagstaff [a]					
S3	−0.0034	0.1461	0.0164	0.1315	251, 251
S4	0.0059	0.0912	0.0089	0.1031	398, 398
S5	0.0040	0.0585	0.0008	0.0721	651, 651
S6	0.0458	0.1052	−0.0335	0.1124	682, 682
S7	0.0635	0.1851	−0.0299	0.2159	450, 450
S8	0.0094	0.0752	−0.0144	0.0801	705, 705
Kiseleva (unpublished)					
S1	−0.0225	0.0601	0.0618	0.0327	3, 3
S2	0.0428	0.0790	0.0009	0.0523	10, 10
S3	0.0061	0.0896	−0.0300	0.1058	19, 19
S4	−0.0152	0.0794	−0.0495	0.1321	20, 20
S5	0.0107	0.0581	−0.0109	0.0700	21, 21
S6	−0.0208	0.0822	−0.0323	0.0945	25, 25
S8	0.0093	0.0903	0.1847	0.1637	13, 13
PHESAT					
S1	−0.0653	0.0649	−0.0073	0.0099	4, 4
S2	0.0009	0.0203	0.0046	0.0103	14, 14
S3	−0.0021	0.0152	0.0027	0.0180	53, 53
S4	0.0002	0.0281	0.0024	0.0180	34, 34
S5	0.0072	0.0179	−0.0005	0.0289	23, 23
S6	0.0010	0.0018	0.0100	0.0272	3, 3

Notes. μ and σ denote, respectively, the mean and standard deviation of the residuals computed in right ascension $\alpha.\cos(\delta)$ and declination δ. N_α and N_δ are the number of observations considered for the respective coordinate. We recall that 0.1 s of arc corresponds to about 600 km at the Saturn distance.
[a] http://www.nofs.navy.mil/data/plansat.html

et al. 2007)

$$\boldsymbol{F}^T_{\hat{i}\hat{k}} = -\frac{3k_2 G m_l^2 R^5 \Delta t}{r_{kl}^8}\left(\frac{2\boldsymbol{r}_{kl}(\boldsymbol{r}_{kl}\cdot\boldsymbol{v}_{kl})}{r_{kl}^2} + (\boldsymbol{r}_{kl}\times\boldsymbol{\Omega}+\boldsymbol{v}_{kl})\right), \tag{2}$$

where $\boldsymbol{r}_{kl} = \boldsymbol{r}_k - \boldsymbol{r}_l$ and $\boldsymbol{v}_{kl} = d\boldsymbol{r}_{kl}/dt$, with $\boldsymbol{\Omega}$, R, and Δt being the instantaneous rotation vector, equatorial radius, and time potential lag of P_k, respectively. The usual tidal term independent of Q (and so only dependent on k_2) that arises in the tidal potential development has been neglected here. This is justified for two reasons: it is pretty small (a typical drift of a few tens of km in longitude after 100 years), and most importantly, since it provides only secular drift (but not secular acceleration) on longitudes, it can easily be absorbed in a tiny change of the initial conditions without any significant consequences. While it was considered only for completeness in Lainey et al. (2009), it has been neglected here.

The time lag Δt is defined by (Lainey et al. 2007)

$$\Delta t = T\ \arctan(1/Q)/2\pi, \tag{3}$$

where T is the period of the main tidal excitation. For the tides raised on Enceladus, T is equal to $2\pi/n$ (n being Enceladus' mean motion) as we only considered the tide raised by Saturn. For Saturn's tidal dissipation, T is equal to $2\pi/2(\Omega - n_i)$, where Ω is the spin frequency of Saturn and n_i is the mean motion of the tide raising Saturnian moon P_i. Δt depends on the tidal frequency and on Q; therefore, it is not a constant parameter.

It is clear from the second term on the right-hand side of Equations (2) and (3) that k_2 and Q are completely correlated. In practice, we considered the commonly used value $k_2 = 0.341$ (Gavrilov & Zharkov 1977) and fitted only Q.

Because of a 2:1 resonance located at the outer edge of the B-ring, Saturn's rings are expected to interact significantly with Mimas (Lissauer & Cuzzi 1982). However the magnitude of this effect is unknown, because of large uncertainties about the ring structures and surface densities. To take into account such an interaction, we had to introduce a supplementary force in the system modeling a constant rate da/dt on Mimas' semi-major axis (denoted by a) and considered as an additional free parameter in the model. As a consequence, no information on tidal dissipation inside Saturn may be obtained directly from Mimas' orbital motion, since the latter is mixed with the estimation of the ring dynamical effects. Moreover, because of the Mimas–Tethys resonant interaction, such a da/dt rate should not be compared with a possible observed kinematic rate. To introduce a da/dt constant term as a supplementary force in the model, we used the Gauss equations. We recall that this differential system provides the variation of Keplerian elements as a function of disturbing forces expressed in the local base. Introducing a constant variation in the semi-major axis (and no variations in the other Keplerian elements), this system can easily be inverted to provide the proper expression of the force.

For an unspecified parameter c_l of the model that shall be fitted (e.g., $\boldsymbol{r}(t_0)$, $d\boldsymbol{r}/dt(t_0)$, Q, ...), a useful relation is

$$\frac{\partial}{\partial c_l}\left(\frac{d^2\boldsymbol{r}_i}{dt^2}\right) = \frac{1}{m_i}\left[\sum_j\left(\frac{\partial \boldsymbol{F}_i}{\partial \boldsymbol{r}_j}\frac{\partial \boldsymbol{r}_j}{\partial c_l} + \frac{\partial \boldsymbol{F}_i}{\partial \dot{\boldsymbol{r}}_j}\frac{\partial \dot{\boldsymbol{r}}_j}{\partial c_l}\right) + \frac{\partial \boldsymbol{F}_i}{\partial c_l}\right], \tag{4}$$

Table 2
Statistics of the Astrometric Residuals Computed from Our Model (Enceladus Tidal Equilibrium Solution) in Arcseconds

Observation subset	ν_s	σ_s	ν_p	σ_p	N_s, N_p
All Observations					
S1	0.0140	0.1027	0.0131	0.1152	1285, 1298
S2	−0.0032	0.0988	0.0048	0.1069	2640, 2643
S3	0.0157	0.1130	−0.0003	0.1152	4702, 4700
S4	0.0150	0.1045	0.0023	0.1096	3775, 3776
S5	0.0113	0.1088	0.0030	0.1151	4471, 4489
S6	0.0238	0.0937	−0.0049	0.1084	2842, 2836
S7	0.0017	0.3275	0.1068	0.4838	138, 113
S8	0.0179	0.0766	0.0076	0.1246	1098, 1101
Struve (1898) 61/62					
S1	0.0076	0.1756	0.0394	0.1810	105, 119
S2	−0.0011	0.1129	−0.0215	0.1170	218, 226
S3	0.0617	0.1363	−0.0185	0.1190	276, 281
S4	0.0671	0.1367	−0.0242	0.1252	167, 170
S8	0.0531	0.0562	−0.0140	0.1181	6, 6
Struve (1898) 21/22					
S7	0.0017	0.3275	0.1068	0.4838	138, 113
S8	−0.0930	0.2411	−0.0063	0.5614	4, 4
Struve (1898)					
S5	−0.1310	0.1191	0.1167	0.0953	44, 42
S6	0.0339	0.1579	0.1721	0.1457	57, 54
Stone (1895)					
S2	−0.0725	0.1892	−0.0533	0.1717	5, 5
S3	−0.0654	0.1987	−0.0908	0.1791	16, 18
S4	−0.0730	0.1514	0.0623	0.1837	17, 19
S5	0.0051	0.0761	−0.0449	0.2588	6, 6
S6	0.0750	0.0000	0.0126	0.0998	1, 2
Stone (1896)					
S5	−0.0569	0.2756	−0.0047	0.1999	54, 75
Stone (1898a, 1898b)					
S3	−0.1127	0.2733	−0.0086	0.2037	12, 12
S4	−0.1519	0.2589	−0.0089	0.2315	30, 28
S5	−0.1048	0.2048	0.0396	0.1578	15, 15
S6	0.0450	0.4001	0.1994	0.2881	4, 4
Morgan (1900)					
S3	0.2297	0.2526	0.0193	0.1762	7, 6
S4	0.3666	0.3065	0.0112	0.1027	6, 4
S5	0.5270	0.2765	0.0594	0.1558	6, 6
Aitken (1905)					
S2	−0.0412	0.2110	0.0744	0.1370	13, 13
S3	0.2097	0.2004	0.0387	0.2382	13, 12
S4	0.2498	0.1967	0.0827	0.2026	13, 13
Barnard (1910)					
S1	−0.0255	0.0989	0.0462	0.1269	6, 3
S2	−0.0721	0.1794	0.0584	0.0769	18, 8
S3	0.0411	0.2075	−0.0668	0.0723	12, 6
S4	0.0642	0.1755	0.0328	0.0913	7, 4
S5	0.0491	0.1116	0.1287	0.2496	8, 6
Aitken (1909)					
S2	−0.0910	0.1515	0.0621	0.0837	7, 8
S3	0.2377	0.2044	0.0678	0.1255	6, 9
S4	0.0847	0.1824	0.0562	0.1178	8, 8
USNO (1929)					
S2	0.0442	0.1108	0.0701	0.0363	2, 2
S3	0.0755	0.1692	−0.0128	0.1869	187, 191
S4	0.0521	0.1356	0.0074	0.1511	158, 157
S5	0.0649	0.1719	0.0174	0.1573	318, 320
S6	0.0996	0.1719	0.0106	0.1482	370, 372
S8	0.1215	0.1606	−0.0088	0.2598	117, 120
Barnard (1913)					
S1	0.1750	0.1093	0.0451	0.0186	3, 3

Table 2
(Continued)

Observation subset	ν_s	σ_s	ν_p	σ_p	N_s, N_p
S2	0.0726	0.1589	0.1242	0.2092	23, 23
S3	0.0804	0.2407	0.0768	0.3137	45, 44
S4	0.0519	0.1929	0.0711	0.3099	33, 33
S5	0.0718	0.2587	0.1386	0.2770	11, 11
Barnard (1915)					
S1	0.1383	0.0890	0.2791	0.3066	3, 4
S2	0.0943	0.1738	0.0023	0.2385	13, 13
S3	0.1256	0.1983	0.0580	0.2757	26, 28
S4	0.1291	0.2024	0.2029	0.2359	23, 23
S5	−0.0554	0.1118	0.0968	0.1420	11, 11
S8	0.3823	0.0000	0.1694	0.0000	1, 1
Barnard (1916)					
S1	0.1941	0.1928	0.0563	0.1434	13, 13
S2	0.0822	0.1972	0.1071	0.2209	19, 19
S3	0.1344	0.1686	0.0225	0.1796	42, 41
S4	0.1946	0.1835	0.0077	0.3271	21, 20
S5	0.1185	0.2452	0.0232	0.2104	12, 12
Barnard (1918)					
S1	−0.0194	0.1599	0.0703	0.0947	7, 6
S2	0.0826	0.2060	0.1282	0.2910	23, 23
S3	0.1649	0.1274	−0.0272	0.1748	36, 35
S4	0.1739	0.1307	−0.0074	0.2939	28, 30
S5	0.2478	0.1294	0.0212	0.3503	10, 9
Barnard (1927)					
S1	0.0125	0.2915	0.1242	0.2063	17, 19
S2	0.0116	0.2274	0.0690	0.2099	65, 66
S3	0.1270	0.1866	0.0215	0.1839	133, 125
S4	0.0936	0.1778	0.0155	0.2015	61, 63
S5	0.1839	0.1887	0.0147	0.3278	45, 43
S8	0.0901	0.2952	0.0284	0.2628	8, 8
Struve (1933) Johannesb					
S1	−0.0016	0.1646	−0.0010	0.1896	115, 115
S2	0.0429	0.1265	−0.0113	0.1324	187, 190
S3	0.0459	0.1249	0.0309	0.1298	127, 130
S4	0.0331	0.1229	0.1023	0.1136	54, 54
S5	−0.0166	0.0268	−0.0740	0.1009	2, 2
USNO (1954) 61/62					
S1	0.0000	0.0000	0.0000	0.0000	0, 0
S2	0.0827	0.1310	−0.0510	0.1843	18, 18
S3	0.0478	0.2775	−0.0200	0.2730	278, 276
S4	0.0732	0.2193	−0.0071	0.1963	283, 284
S5	0.0591	0.2203	0.0175	0.2220	455, 457
S6	0.0572	0.1785	−0.0466	0.1737	194, 188
S8	−0.0839	0.0000	−0.0360	0.0000	1, 1
Struve (1933) Yerkes					
S2	−0.1751	0.2256	0.0512	0.2054	48, 48
USNO (1954)					
S5	−0.0007	0.1547	0.0172	0.0857	32, 32
S6	0.0007	0.1547	−0.0172	0.0857	32, 32
Harper et al. (1997)					
S3	−0.0079	0.0377	0.0090	0.0602	184, 184
S4	−0.0024	0.0318	−0.0053	0.0580	193, 193
S5	0.0016	0.0281	−0.0025	0.0545	202, 202
S6	0.0062	0.0213	−0.0157	0.0682	118, 118
S8	−0.0023	0.0451	0.0049	0.0708	51, 51
Qiao et al. (1999)					
S1	−0.0448	0.1181	0.0086	0.0174	15, 15
S2	−0.0454	0.0802	0.0060	0.0645	47, 47
S3	−0.0065	0.0423	0.0050	0.0564	82, 82
S4	−0.0037	0.0296	−0.0017	0.0423	147, 147
S5	0.0088	0.0368	−0.0050	0.0477	151, 151
S6	−0.0017	0.0265	−0.0076	0.0578	164, 164

Table 2
(Continued)

Observation subset:	ν_s	σ_s	ν_p	σ_p	N_s, N_p
Veiga et al. (2003)					
S1	−0.0046	0.0534	−0.0059	0.0704	329, 329
S2	0.0069	0.0613	−0.0038	0.0720	414, 414
S3	−0.0041	0.0430	0.0103	0.0710	489, 489
S4	0.0055	0.0522	−0.0064	0.0721	527, 527
S5	−0.0106	0.0451	−0.0106	0.0947	480, 480
S6	0.0293	0.0583	0.0270	0.0932	219, 219
S8	−0.0339	0.0217	−0.1685	0.0502	7, 7
Vienne et al. (2001)					
S1	0.0439	0.0347	0.0103	0.0345	216, 216
S2	−0.0017	0.0421	0.0051	0.0513	860, 860
S3	−0.0050	0.0264	−0.0052	0.0396	1747, 1747
S4	0.0033	0.0247	0.0060	0.0377	1029, 1029
S5	−0.0018	0.0230	−0.0046	0.0507	1587, 1587
S6	0.0001	0.0153	−0.0006	0.0405	731, 731
S8	0.0036	0.0291	0.0061	0.0643	523, 523
Harper et al. (1999)					
S3	−0.0017	0.0272	−0.0106	0.0497	245, 245
S4	−0.0222	0.0400	0.0114	0.1133	205, 205
S5	0.0055	0.0423	0.0059	0.0856	238, 238
S6	0.0133	0.0351	−0.0135	0.0534	242, 242
S8	0.0076	0.0243	0.0083	0.0383	188, 188
Peng et al. (2002)					
S1	−0.0139	0.0302	0.0390	0.0485	54, 54
S2	−0.0181	0.0273	0.0062	0.0438	161, 161
S3	0.0093	0.0226	0.0053	0.0281	145, 145
S4	−0.0006	0.0182	−0.0022	0.0304	161, 161
S5	0.0068	0.0237	0.0055	0.0295	199, 199
S6	−0.0010	0.0126	−0.0005	0.0505	145, 145
S8	−0.0027	0.0191	−0.0281	0.0527	126, 126
Qiao et al. (2004)					
S1	−0.0400	0.1096	0.0466	0.1996	44, 44
S2	−0.0682	0.1322	−0.0005	0.2055	141, 141
S3	−0.0091	0.0866	0.0189	0.1497	236, 236
S4	−0.0175	0.0733	−0.0230	0.0987	246, 246
S5	0.0174	0.0571	−0.0001	0.1237	227, 227
S6	0.0232	0.0401	−0.0514	0.1428	207, 207
S8	0.0291	0.0274	0.1340	0.1958	66, 66
Peng et al. (2008)					
S1	0.0256	0.0712	0.0082	0.0912	358, 358
S2	−0.0009	0.0260	−0.0003	0.0383	358, 358
S3	−0.0051	0.0234	0.0007	0.0296	358, 358
S4	−0.0056	0.0237	−0.0003	0.0325	358, 358
S5	−0.0082	0.0245	0.0021	0.0418	358, 358
S6	0.0074	0.0209	−0.0200	0.1202	358, 358

Notes. μ and σ denote, respectively, the mean and standard deviation of the residuals computed in separation s and position angle p. N_s and N_p are the number of observations considered for the respective coordinate. We recall that 0.1 s of arc corresponds to about 600 km at the Saturn distance.

where $\boldsymbol{F}_i$ is the right-hand side of Equation (1) multiplied by m_i.

Partial derivatives of the solutions with respect to initial positions and velocities of the satellites and dynamical parameters are computed from simultaneous integration of Equation (4) and Equation (1). For an explicit formulation of the dynamical equations and the variational equations used, we refer to Lainey et al. (2007, 2009), Lainey (2008), and references therein.

The RA15 numerical integrator is used with a constant step size of 0.075 days. To increase the numerical accuracy, we performed forward and backward integrations starting at an initial Julian epoch of 2,433,291.0 (1950 January 9, TDB). The numerical accuracy of our simulation is at the level of a few hundreds of meters over the whole 123 years (see also Appendix A.1.1).

During the fitting procedure, timescale and light-time corrections for each satellite-observer distance were introduced (Lainey et al. 2007). Corrections for phase, aberration, and differential refraction were applied when they were not already included in the observation astrometric reductions (Lainey et al. 2007). Observational subsets (related to different observational campaigns or publications) have been considered with a

relative weight computed by preliminary residuals (Lainey et al. 2007) and corresponding to their rms error for deriving formal errors. Least-squares iterations have been applied to solve for the fitted parameters. In particular, despite the development of new techniques, least squares is still one of the most efficient methods available to solve for the parameters of dynamical systems (Desmars et al. 2009a), as long as the studied system has been observed over a sufficiently long period of time to allow for rather accurate initial conditions (which is the case for the main planetary satellites of the solar system). No constraints have been applied in the least-squares inversion. Only a few iterations have been required to reach an optimal solution.

In all this work, the fitted parameters are the initial state vectors of the main Saturnian moons (actually their equivalent form as Keplerian elements) of all Saturnian moons, the extra parameter da/dt for Mimas and the ratio k_2/Q for Saturn. In particular, Enceladus' tidal dissipation could not be fitted due to significant correlations. To solve this issue, we considered two extreme scenarios for each solution: (1) Enceladus is at thermal equilibrium and (2) Enceladus is not dissipative at all. Then we merged both solutions into one, providing one global solution with higher error bars, but independent of Enceladus' internal state (see Section 4). Hence, the total number of fitted parameters considered is between 50 and 53 (depending on whether Q is assumed constant or dependent on the tidal frequency).

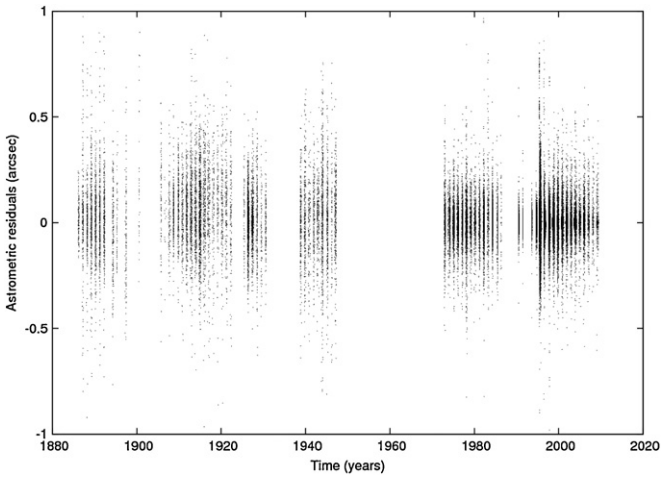

Figure 1. Astrometric residuals. Residuals between the astrometric observations and our numerical model (assuming eccentricity equilibrium for Enceladus), after fitting the initial state vectors of the eight main Saturnian moons, the ratio k_2/Q of Saturn and a constant rate da/dt on Mimas' semi-major axis. The global 1σ accuracy is about 0.1 arcsec (we recall that at the Saturnian distance 1 arcsec corresponds to about 6000 km). It can be noted that no clear differences between old and modern observations are obvious due to (1) selective criteria in precision for all subsets (see Section 2 for details) and (2) limitations inherent in graphical resolution (see Tables 1 and 2 for a detailed analysis of each observation subset).

4. FITTING THE MODEL TO ASTROMETRIC OBSERVATIONS

The dependence of Q on tidal frequency is a matter for debate. While it is traditionally approximated by a constant for long timescales (Goldreich & Soter 1966; Sinclair 1983), recent developments in the numerical simulation of giant planet interiors have revealed a possible erratic frequency dependence of Q (Wu 2005). In this work we investigate both possibilities.

4.1. Constant Q Model

In a first inversion, we neglect dissipation in Enceladus and fit the initial state vectors of all eight moons including Saturn's ratio k_2/Q and Mimas' da/dt. We thus obtain $k_2/Q = (2.0 \pm 0.4) \times 10^{-4}$ and $da/dt = -(13.7 \pm 2.4) \times 10^{-15}$ AU day^{-1}. Saturn's dissipation ratio corresponds to orbital acceleration values $\dot{n}/n$ (in yr^{-1} units) of $-(2.67 \pm 0.57) \times 10^{-10}$, $-(4.26 \pm 0.91) \times 10^{-10}$, $-(1.52 \pm 0.33) \times 10^{-10}$, and $-(3.56 \pm 0.76) \times 10^{-11}$ for Enceladus, Tethys, Dione, and Rhea, respectively. This translates into semi-major axis variation da/dt (in au day^{-1} units) of $(7.77 \pm 1.67) \times 10^{-16}$, $(1.53 \pm 0.33) \times 10^{-15}$, $(7.02 \pm 1.50) \times 10^{-16}$, and $(2.29 \pm 0.49) \times 10^{-16}$. Over the 123 years covered by the observation set we used, this corresponds to an orbital shift in longitude of 799 ± 172 km (0.129 ± 0.028 arcsec), 1152 ± 246 km (0.186 ± 0.040 arcsec), 365 ± 78 km (0.059 ± 0.013 arcsec), and 72 ± 15 km (0.012 ± 0.002 arcsec), respectively. In a second case, we introduce dissipation in Enceladus, which is expected to counterbalance its orbital acceleration, thereby modifying our global estimation of Saturn k_2/Q obtained from the satellite tidal accelerations. As already stated in Section 3, we do not have a sufficient number of observations to invert independently the k_2/Q values for Saturn and Enceladus. Hence, to introduce Enceladus' tidal dissipation, we assume that Enceladus is in a dynamical equilibrium state, which locks Enceladus' eccentricity as the result of dissipation in both Saturn and Enceladus inside the 2:1 resonance with Dione (Meyer & Wisdom 2007). In this case, we obtain $k_2/Q = (2.6 \pm 0.4) \times 10^{-4}$ and $da/dt = -(17.0 \pm 2.4) \times 10^{-15}$ AU day^{-1}. The associated secular accelerations related to Saturn's and Enceladus' tides are $-(2.06 \pm 0.57) \times 10^{-10}$, $-(5.61 \pm 0.91) \times 10^{-10}$, $-(2.09 \pm 0.32) \times 10^{-10}$, $-(4.69 \pm 0.76) \times 10^{-11}$. This translates into semi-major axis variation da/dt (in AU day^{-1} units) of $(6.00 \pm 1.66) \times 10^{-16}$, $(2.02 \pm 0.33) \times 10^{-15}$, $(9.65 \pm 1.49) \times 10^{-16}$, and $(3.02 \pm 0.49) \times 10^{-16}$. This corresponds to 619 ± 171 km (0.100 ± 0.028 arcsec), 1516 ± 245 km (0.245 ± 0.040 arcsec), 501 ± 78 km (0.081 ± 0.013 arcsec), and 95 ± 15 km (0.015 ± 0.002 arcsec), as well. Even though both inversions provide the same orbital trends, acceleration values for each satellite are somewhat different. This arises from the use of only one global k_2/Q value for Saturn, while fitting several independent accelerations. Thanks to the long time span considered, astrometric accuracy is enough to detect tidal accelerations for Enceladus, Tethys, Dione, and Rhea from the observations (see Figure 1 and Tables 1–3). Combining the two fits, our nominal solution for the Saturn tidal dissipation (here assumed to be independent of the tidal frequency) yields $k_2/Q = (2.3 \pm 0.7) \times 10^{-4}$.

4.2. Non-constant Q Model

To check the assumption of a constant Q model considered in our nominal solution, we release simultaneously several Q values (with and without Enceladus' dissipation), one Q value being related to each tide-raising satellite. We succeed in obtaining Saturn's Q at four different tidal frequencies, related to Enceladus, Tethys, Dione, and Rhea (see Figure 2), respectively. Correlations between the four tidal ratios are below 0.2 (as shown in Table 4). However, a high correlation of 0.935 is found between Saturn's tidal ratio associated with Tethys' tidal frequency and Mimas' da/dt (equal to $-(16.3 \pm 3.7) \times 10^{-15}$ AU day^{-1}), as a consequence of the 2:4 mean motion resonance between Mimas and Tethys.

Implications of these results are discussed in Section 6.

Table 3
Correlation between k_2/Q and da/dt with All Our Fitted Parameters (Enceladus Tidal Equilibrium Solution)

	a_1	l_1	k_1	h_1	q_1	p_1	a_2	l_2	k_2	h_2	q_2	p_2
k_2/Q	−0.116	0.142	0.103	−0.012	−0.031	−0.309	−0.035	0.705	0.000	0.484	0.000	−0.010
da/dt	0.085	−0.020	−0.125	−0.044	0.082	0.375	0.027	−0.588	−0.005	−0.415	0.011	0.008
	a_3	l_3	k_3	h_3	q_3	p_3	a_4	l_4	k_4	h_4	q_4	p_4
k_2/Q	−0.043	0.169	0.014	−0.037	−0.199	0.219	−0.170	0.372	0.088	−0.070	0.036	−0.027
da/dt	0.087	0.241	−0.054	0.046	0.247	−0.290	0.157	−0.303	−0.076	0.066	−0.045	0.042
	a_5	l_5	k_5	h_5	q_5	p_5	a_6	l_6	k_6	h_6	q_6	p_6
k_2/Q	0.032	0.136	0.028	−0.030	−0.016	0.022	0.052	0.014	−0.004	0.018	0.014	−0.019
da/dt	0.007	−0.106	−0.026	0.009	0.012	−0.017	0.035	−0.011	−0.001	−0.014	−0.010	0.012
	a_7	l_7	k_7	h_7	q_7	p_7	a_8	l_8	k_8	h_8	q_8	p_8
k_2/Q	−0.001	0.005	0.001	0.000	−0.004	−0.014	−0.016	−0.014	0.000	0.008	0.001	−0.031
da/dt	0.001	−0.004	−0.002	0.000	0.003	0.009	0.023	0.013	0.001	−0.024	−0.002	0.024
	k_2/Q	da/dt										
k_2/Q	1.000	−0.838										
da/dt	−0.838	1.000										

Notes. Where a is the semi-major axis, l is the mean longitude, $k = e.\cos(\Omega + \omega)$, $h = e.\sin(\Omega + \omega)$, $q = \sin(i/2).\cos(\Omega)$ and $p = \sin(i/2).\sin(\Omega)$ (with e denoting the eccentricity, Ω denoting the longitude of the node, and ω denoting the argument of the periapsis). Numbers 1, . . ., 8 refer to Mimas (S1), . . ., Iapetus (S8), respectively.

Table 4
Correlation between All Four k_2/Q Ratios Estimated at the Tidal Frequency of Enceladus, Tethys, Dione, and Rhea, and da/dt (Enceladus' Eccentricity Equilibrium Solution)

	$k_2/Q(S_2)$	$k_2/Q(S_3)$	$k_2/Q(S_4)$	$k_2/Q(S_5)$	da/dt
$k_2/Q(S_2)$	1.000	0.020	−0.197	0.003	−0.012
$k_2/Q(S_3)$	0.020	1.000	0.001	0.000	−0.935
$k_2/Q(S_4)$	−0.197	0.001	1.000	0.024	0.004
$k_2/Q(S_5)$	0.003	0.000	0.024	1.000	0.006
da/dt	−0.012	−0.935	0.004	0.006	1.000

5. ROBUSTNESS OF THE SOLUTION

In this section, we present various tests that assess the robustness of our solution. During these tests, we considered as a reference solution the Enceladus equilibrium scenario with a constant Saturn Q model, that is, $k_2/Q = (2.6 \pm 0.4) \times 10^{-4}$ and $da/dt = -(16.9 \pm 2.4) \times 10^{-15}$ AU day^{-1}.

5.1. Random Holdout Method

This method considers the change in fitted parameters when a constant percentage of observations is removed. We have performed a test, with a percentage of 10% of observations that are not used. The number of observations in the full nominal least-squares inversion is 19,616 (all moon coordinates at a given time considered as one observation). One hundred different subsets were generated and used to check the robustness of the fitted parameters. We obtained the k_2/Q-value in the interval $[1.8 \times 10^{-4}, 3.3 \times 10^{-4}]$ for Saturn and the Mimas da/dt value in the interval $[-21.9 \times 10^{-15}, -9.1 \times 10^{-15}]$ AU day^{-1} (even though most values were in agreement with the nominal error bars). This suggests that factors of two and four could be introduced in our nominal error bars in k_2/Q and da/dt, respectively. However, it must be remembered that Mimas and Tethys are hard to observe from the ground. Hence, significantly decreasing the number of observations of Mimas will automatically increase the chance of losing the da/dt signal.

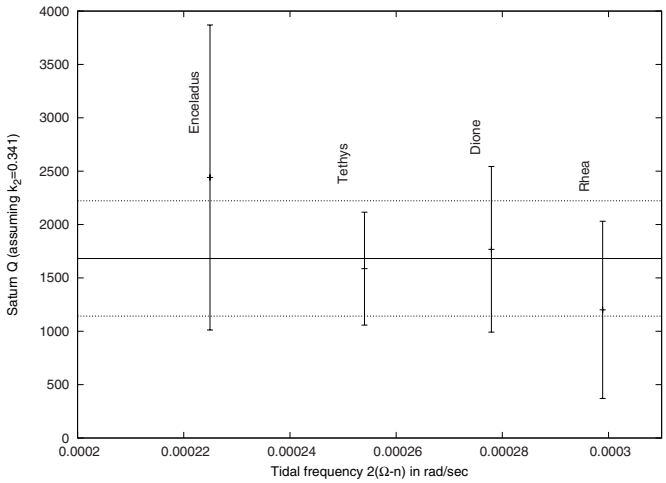

Figure 2. Determination of the Saturn tidal dissipation factor Q. Saturn's tidal dissipation factor Q vs. the tidal frequency $2(\Omega - n)$, where Ω and n denote its rotation rate and the moon mean motion, respectively. The Love number is assumed to be $k_2 = 0.341$. The horizontal line shows the nominal solution (constant Q model) equal to $Q = 1682 \pm 540$, with error bars as dashed lines. The vertical values with error bars are derived from a variable Q model. The large error bar associated with Enceladus is a consequence of the uncertain tidal dissipation in that satellite (whether one assumes no dissipation or eccentricity equilibrium). Presumably, the small value of Q is the signature of a rock–ice core or its boundary in Saturn.

5.2. Removing Successively the Five Largest Observation Subsets

In this test, we completely removed several observation subsets among the most dense ones: (1) Vienne et al. (2001), (2) Vass (1997), (3) FASTT observations (see Stone & Harris 2000, and references therin), (4) Struve (1898), and (5) USNO

Table 5
Fitted Value of k_2/Q and da/dt after Removing Observation Subsets

Subset Removed	k_2/Q	da/dt (AU day^{-1})	Observations
Vienne et al. (2001)	$(2.0 \pm 0.4) \times 10^{-4}$	$-(11.0 \pm 2.4) \times 10^{-15}$	6693
Vass (1997)	$(2.6 \pm 0.4) \times 10^{-4}$	$-(16.9 \pm 2.3) \times 10^{-15}$	3977
FASTT	$(2.6 \pm 0.4) \times 10^{-4}$	$-(16.9 \pm 2.3) \times 10^{-15}$	3137
Struve (1898)	$(4.2 \pm 0.6) \times 10^{-4}$	$-(20.8 \pm 2.9) \times 10^{-15}$	796
USNO (1929)	$(2.6 \pm 0.5) \times 10^{-4}$	$-(12.9 \pm 2.5) \times 10^{-15}$	1162

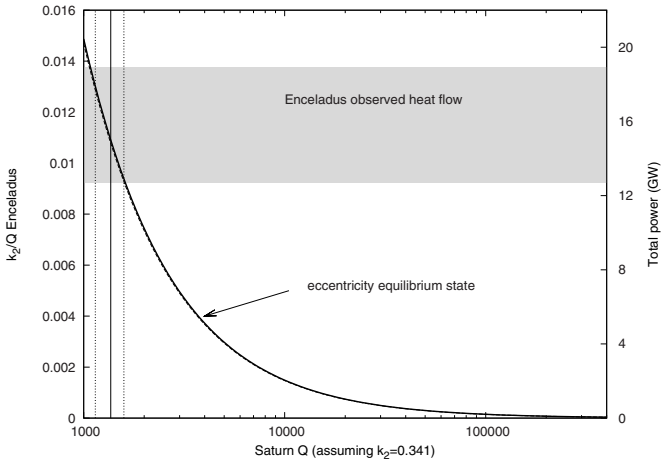

Figure 3. Comparison of Enceladus' thermal emission power with the Saturn tidal dissipation determined in the present study. The solid curve indicates the k_2/Q ratio and total dissipated power (in GW) in Enceladus for which the current orbital configuration of Enceladus and Dione is at eccentricity equilibrium as a function of Q in Saturn. Assuming such equilibrium in our fit, the value of Saturn's Q that we derive ($Q = 1363 \pm 221$; see the vertical line with associated dashed lines for error bars) shows that the expected total heat production rate is close to the observed emitted power. Hence, tidal heating equilibrium is a possible mechanism for maintaining Enceladus' thermal activity at its currently observed rate.

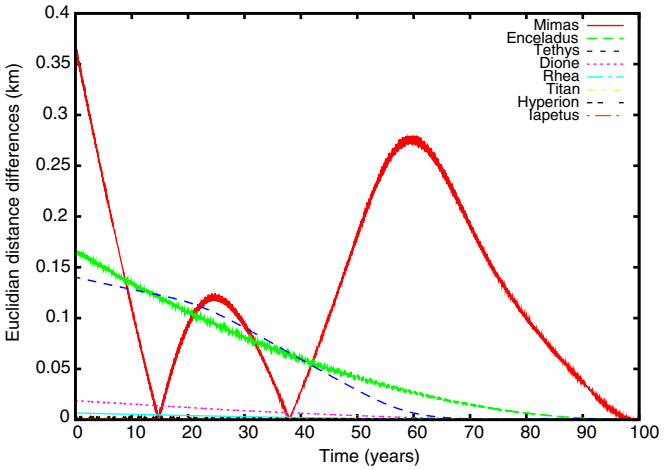

Figure 4. Test of the numerical precision of our model using the forward-backward method.
(A color version of this figure is available in the online journal.)

(1929). The first three observation subsets are associated with the modern era, while the last two consist of observations from the end of the 19th century and beginning of the 20th century, respectively. We provide in Table 5 the fitted value of k_2/Q and da/dt after having removed the mentioned subset.

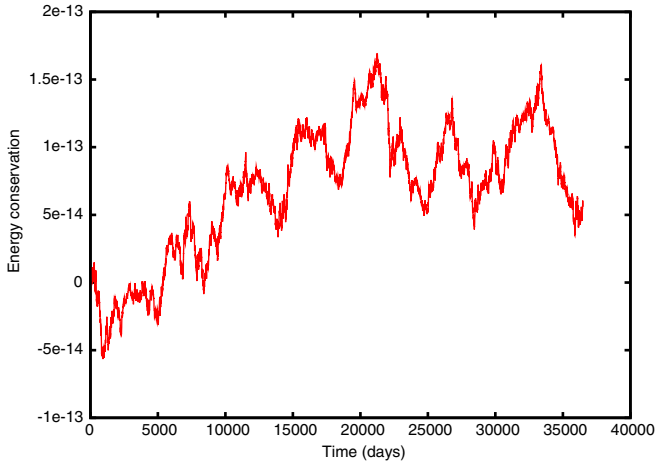

Figure 5. Energy conservation within our model (see the text for details).
(A color version of this figure is available in the online journal.)

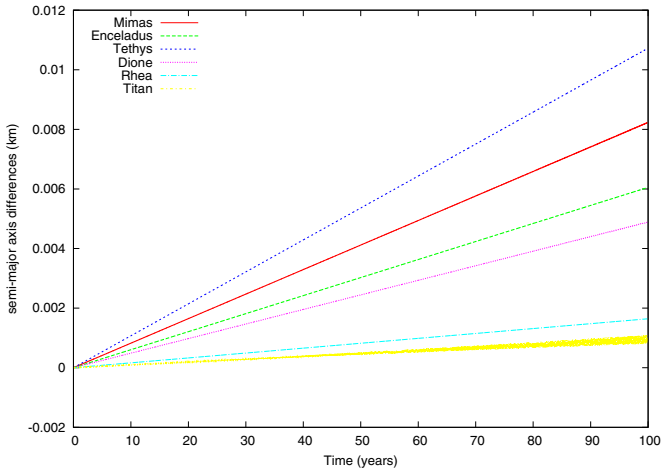

Figure 6. Semi-major axis variation test under the effect of tides raised in the planet (two-body problem).
(A color version of this figure is available in the online journal.)

With the exception of removing the Struve data, all solutions above are very close to (though not in full agreement with) our nominal solution. The Struve data even indicate a slightly higher tidal dissipation ratio. We conclude that removing any observational subsets (old or modern) still confirms the high Saturnian dissipation obtained in our nominal solution.

5.3. On the Use of Pixel Positions

As already mentioned in Section 2, the ephemerides of the outermost Saturnian moons are sometimes used to determine the scale and orientation of the observations (because of the lack of stars in the observed fields). This can be justified since outermost

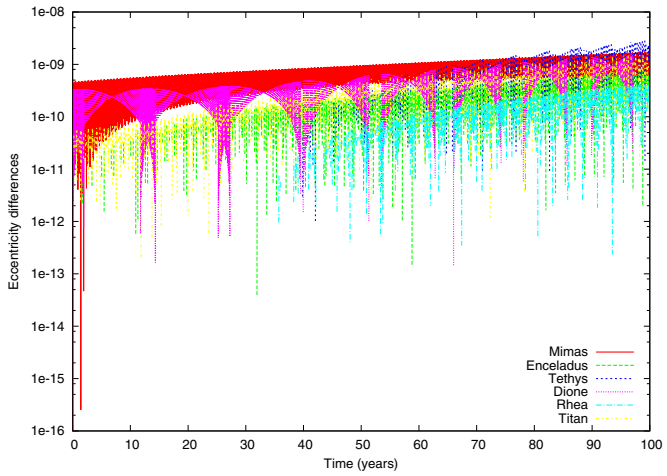

Figure 7. Eccentricity variation test under the effect of tides raised in the planet (two-body problem).

(A color version of this figure is available in the online journal.)

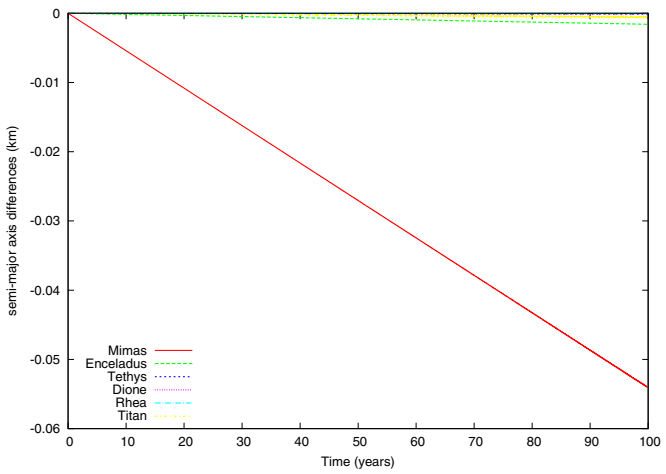

Figure 8. Semi-major axis variation test under the effect of tides raised in the satellites (two-body problem).

(A color version of this figure is available in the online journal.)

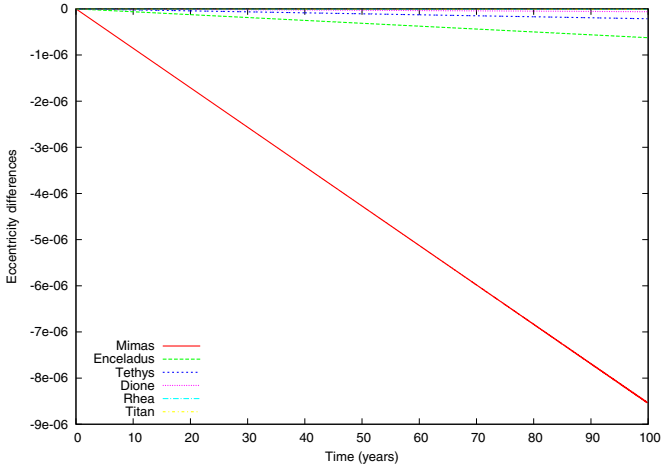

Figure 9. Eccentricity variation test under the effect of tides raised in the satellites (two-body problem).

(A color version of this figure is available in the online journal.)

moons (Dione, Rhea, Titan, and sometimes Iapetus) are easier to observe (entailing a more accurate ephemeris). Moreover, an error on the scale factor and orientation is expected to have a smaller influence on the innermost moons that are close to the center of the observation. Nevertheless, introducing possibly an external orbital model in the reduction of the observations is not fully satisfactory. This is why we decided, when available, to use pixel positions instead of (α, δ) or (s, p) coordinates. Under this form, the observations are not corrupted by any external dynamical model, but their significance in the fit is lower, since information on the scale and orientation is no longer present.

We have checked the difference between our nominal solution (using pixel positions) and a fit using the usual astrometric coordinates (α, δ) or (s, p). We obtained the following result: $k_2/Q = (1.8 \pm 0.4) \times 10^{-4}$ for Saturn and $da/dt = -(13.0 \pm 2.4) \times 10^{-15}$ for Mimas. This is in agreement with our nominal solution (taking into account the error bars).

5.4. Scale Factor Biases

One of the crucial systematic errors in astrometric observations is related to scale factors. Scale factors express the equivalence between an observed distance on a field (measured in micrometer on a photographic plate, or pixel on a CCD image) and its related angular separation on the celestial sphere. In principle, a scale factor should be an isotropic quantity. Nevertheless, stellar positions used to calibrate the observations are rarely corrected for atmospheric differential refraction. Hence, scale factors along equatorial and polar directions are different. Most of the time, old observations used a constant scale factor, which introduced systematic errors in the satellite positions. In particular, such errors produce higher residuals for the distant satellites than for the closer ones, which are much less affected by a small error in the field scale.

To check the influence of scale factor errors on our results, we have performed another fit of our model using this time the relative distance of the satellites between each other (instead of the absolute distance derived from the scale factor estimation), when at least three satellites were observed simultaneously. We obtained the following result: $k_2/Q = (2.7 \pm 0.3) \times 10^{-4}$ for Saturn and $da/dt = -(17.9 \pm 1.8) \times 10^{-15}$ for Mimas. These two values agree with our nominal solution within the error bars.

5.5. Releasing More Parameters in the Fit (Saturn's Pole and Precession)

While the gravity field parameters we are using are accurate thanks to *Cassini* data, the IAU expression for Saturn's pole coordinates and precession frequency dates back to 1994 (Davies et al. 1996; Archinal et al. 2011). Here, we investigate the influence of fitting the pole coordinates and precession frequency of Saturn on our results. Starting from our nominal solution (the Enceladus equilibrium model), we performed a new fit that added four more parameters in the fitting process. These parameters refer to the IAU formulation for the pole coordinates of planets (Archinal et al. 2011):

$$\begin{aligned} \alpha &= \alpha_0 + \dot{\alpha} T \\ \delta &= \delta_0 + \dot{\delta} T \end{aligned} \quad ,$$

where (α_0, δ_0) are the pole coordinates in the ICRF at epoch J2000.0 and $(\dot{\alpha}, \dot{\delta})$ introduces the precession/nutation of the primary. Releasing the $50+4$ parameters simultaneously, we obtain after iterations the following solution: $k_2/Q = (2.63 \pm 0.41) \times 10^{-4}$, $da/dt = -(16.7 \pm 2.4) \times 10^{-15}$ AU day^{-1}, $\alpha_0 = 40.5915 \pm 0.0055^\circ$, $\dot{\alpha} = -0.131 \pm 0.022^\circ$/Julian century,

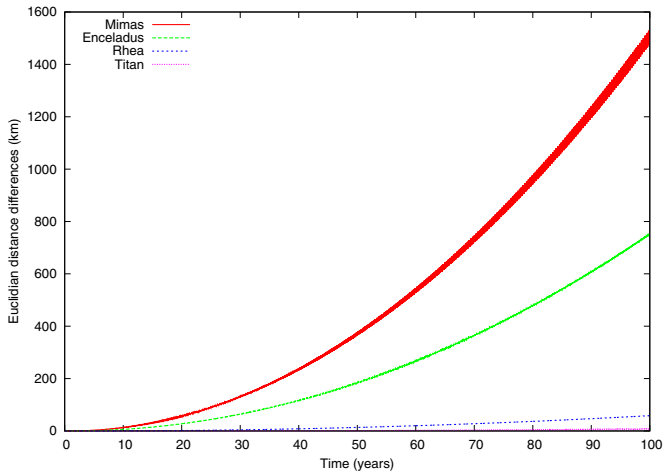

Figure 10. Semi-major axis variation test under the effect of tides raised in the planet (full model).

(A color version of this figure is available in the online journal.)

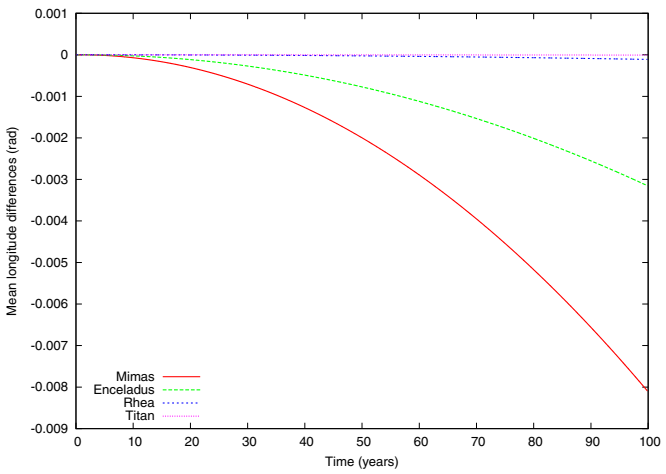

Figure 11. Eccentricity variation test under the effect of tides raised in the planet (full model).

(A color version of this figure is available in the online journal.)

$\delta_0 = 83.54163 \pm 000053^\circ$, $\dot{\delta} = 0.0219 \pm 0.0025^\circ$/Julian century.

Clearly k_2/Q and da/dt are poorly affected by adding to the fit Saturn's pole coordinates and precession frequency. Moreover, the post-fit residuals are highly similar to those from the nominal solutions (in the limit of one-tenth of a mas). Hence, our results are expected to be poorly sensitive to possible IAU errors in the expression of Saturn's pole coordinates and precession frequency.

5.6. Neglecting General Relativity

Here we focus on the influence of general relativity. Since the influence of these effects is pretty small (Iorio & Lainey 2005), they have been neglected in our nominal fits. To demonstrate the validity of such an assumption, we have introduced these effects in the model (we considered relativistic effects associated to both Saturn and the Sun) and performed a new solution. After fitting, we obtained $k_2/Q = (2.54 \pm 0.42) \times 10^{-4}$, $da/dt = -(16.9 \pm 2.4) \times 10^{-15}$ AU day^{-1}.

Here again, the post-fit residuals are highly similar to the nominal solution ones (in the limit of one-tenth of a mas).

In conclusion, the envelope of all the tests performed in this whole section provides $k_2/Q = (3.1 \pm 1.7) \times 10^{-4}$ and $da/dt = -(16.2 \pm 7.6) \times 10^{-15}$ AU day^{-1}. In particular, our different tests confirm that the present estimation of the k_2/Q ratio of Saturn is reliable.

6. DISCUSSION

We can see from Section 4.2 that all k_2/Q values lie in the same range and show smooth frequency dependence. To understand the implications of this result, let us recall what is presently known about the physical mechanisms that convert into heat the kinetic energy of the tides, thus driving the secular evolution of the system. Saturn has a hydrogen–helium fluid envelope, which may be partially or entirely convective, and an expected rock–ice core (Guillot 1999) (ignoring here the role of a possible outer radiative layer). The fluid equilibrium tide is damped mainly in the convective part of the envelope, and its amplitude depends smoothly on frequency (Zahn 1966, 1989). In contrast, the dynamical tide in this region, which consists of excited inertial modes (Ogilvie & Lin 2004; Wu 2005; Goodman & Lackner 2009), varies considerably with frequency, particularly in the presence of a dense core (Rieutord & Valdettaro 2010). Although both of these fluid tides are damped through turbulent friction, they yield a relatively low value of the dissipation parameter: $k_2/Q \sim 10^{-6}$ at most (Ogilvie & Lin 2004). Therefore, one has to turn to other mechanisms to explain the high tidal dissipation in Saturn's system that we report here, with k_2/Q ranging from 1.4×10^{-4} to 3.4×10^{-4}. For instance, the contribution to tidal dissipation of a stably stratified layer surrounding the core, due to the settling of helium when it ceases to be soluble in metallic hydrogen (Morales et al. 2009; Fortney & William 2003), remains to be evaluated. Another possibility could be the presence of a dense core, as predicted by most models (Guillot 1999). In Saturn, this core is expected to be relatively larger than in Jupiter, which would be consistent with the relatively lower tidal dissipation in that planet: $k_2/Q = (1.102 \pm 0.203) \times 10^{-5}$, as determined by the same method (Lainey et al. 2009).

So far, the averaged lower bound of Saturn's Q was derived from theoretical considerations, assuming that all main moons formed above the synchronous orbit 4.5 Byr ago (Goldreich & Soter 1966). Considering Mimas, the innermost mid-sized satellite, and using the averaged equations for a tidally evolving system, Sinclair (1983) derived a present-day reference value of $Q \geqslant 18{,}000$ (assuming $k_2 = 0.341$ from Gavrilov & Zharkov 1977). If the observed high value of Saturn's k_2/Q determined in this work represents well the long-term averaged value, then a very large tidal expansion of the moon orbits should have occurred. In particular, the conventional assumption of Saturnian satellites forming contemporaneously with their parent planet has to be dismissed. Recently, Charnoz et al. (2011) suggested a new mechanism of formation of Saturnian satellites at the outer edge of the rings. While the satellites evolve outward in their model due to exchange of angular momentum with the rings and tides that rose in the primary, they noticed, however, that a strong tidal dissipation in Saturn is mandatory to place the satellites at their current observed positions. It is noteworthy that the tidal dissipation quantification presented here allows their model to form and place the Saturnian satellites at the proper distance to their primary.

Since the discovery of the very active province at Enceladus' south pole by the *Cassini* spacecraft in 2005 (Spencer et al. 2009; Porco et al. 2006), a variety of theoretical models have

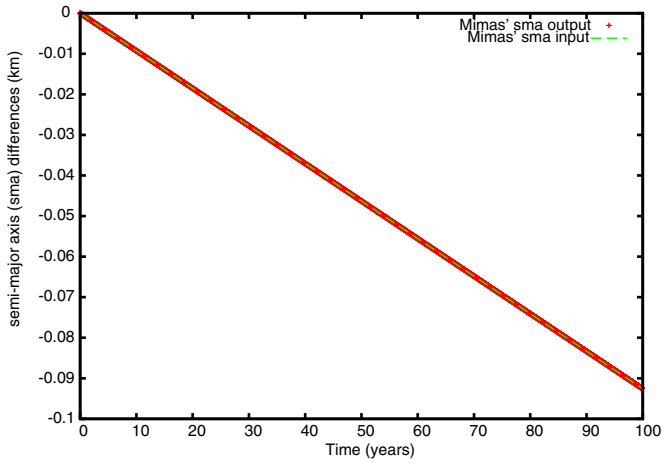

Figure 12. Test of the da/dt perturbation in the two-body problem case.
(A color version of this figure is available in the online journal.)

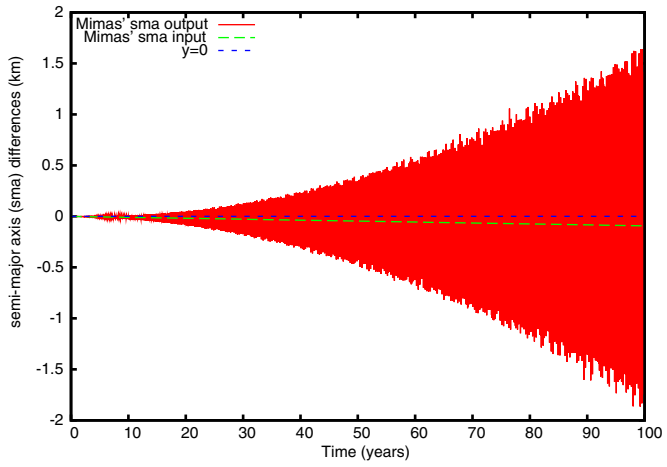

Figure 13. Mimas' semi-major axis variation under the influence of da/dt perturbation (full model).
(A color version of this figure is available in the online journal.)

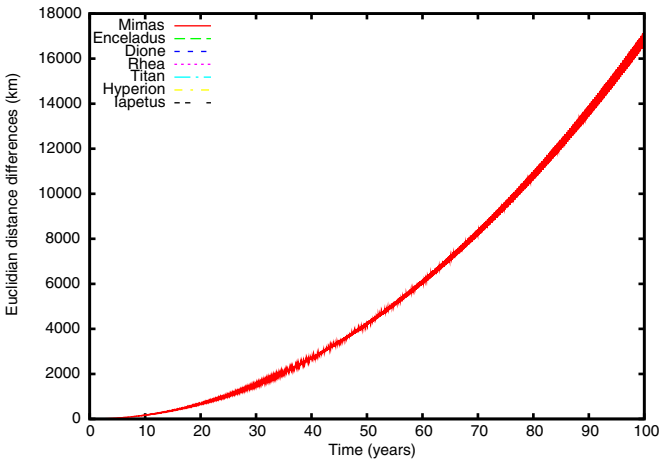

Figure 14. Mimas' orbital position differences under the influence of da/dt perturbation (full model).
(A color version of this figure is available in the online journal.)

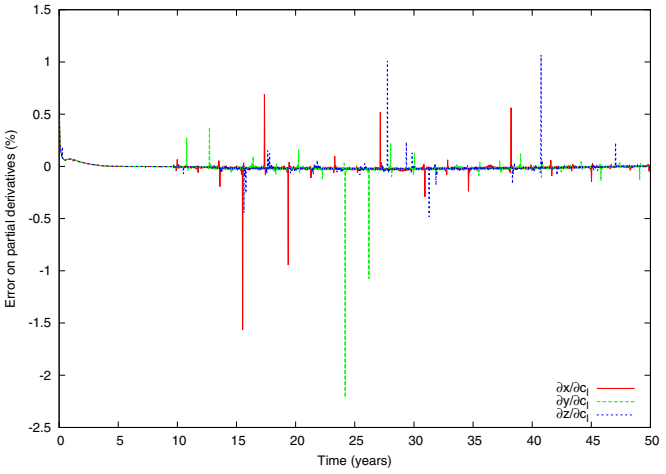

Figure 15. Variational equations test of da/dt parameter from Mimas position.
(A color version of this figure is available in the online journal.)

been proposed to explain the huge thermal emission and the associated eruptions of water vapor and ice particles (Meyer & Wisdom 2007; Nimmo et al. 2007; Tobie et al. 2008; O'Neill & Nimmo 2010; Howett et al. 2011). The amount of energy produced at present by radioactive decay in the rocky core of Enceladus contributes less than 2% to the total emitted power (15.8 ± 3.1 GW; Howett et al. 2011), suggesting another internal energy source such as tidal dissipation. Previous studies based on the former estimation of Saturn's Q ($\geqslant$18,000) (Sinclair 1983) showed that tidal heating at orbital equilibrium, required to maintain the resonant Enceladus–Dione orbital configuration, could not account for more than 1.1 GW (Meyer & Wisdom 2007). This was suggesting that either the resonant system oscillates around equilibrium with dissipated power varying from almost zero to the observed value or more, or the satellite episodically releases the internal heat that is continuously produced at a rate compatible with orbital equilibrium (Tobie et al. 2008; O'Neill & Nimmo 2010). None of these solutions were fully satisfactory.

The new dissipation factor of Saturn reported here totally changes our understanding of Enceladus' heat production mechanism. As shown in Figure 3, with the new inferred Q value, equilibrium tidal heating can now account for the observed heat power. This indicates that Enceladus' interior could be close to thermal equilibrium at present, with surface heat loss being balanced by heat produced by tidal dissipation. Large tidal dissipation in Enceladus implies that the satellite probably possesses a liquid water layer decoupling the outer ice shell from the rocky core (Nimmo et al. 2007; Tobie et al. 2008). For Saturnian Q lower than 2000, Enceladus can remain highly dissipative during a very long period of time without damping its orbital eccentricity, and the long-term stability of a subsurface ocean would thus be possible.

7. CONCLUSION

We have quantified Saturn's tidal dissipation ratio k_2/Q to be $(2.3 \pm 0.7) \times 10^{-4}$ using astrometric observations spanning 123 years. Moreover, such a quantification directly derived from observations is provided here at various frequencies, for the first time in a giant planet. As a consequence, we conclude that tidal dissipation may mostly occur in Saturn's core and its boundary. Moreover, tidal heating equilibrium is now a possible state for Enceladus.

The present quantification of Saturnian tidal dissipation is incompatible with a satellite formation scenario in Saturn's

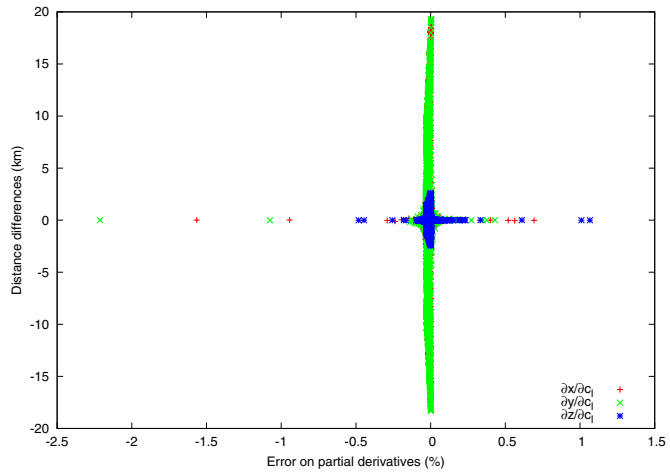

Figure 16. Distribution of distance differences as a function of error on partial derivatives using the test of da/dt parameter from Mimas position.

(A color version of this figure is available in the online journal.)

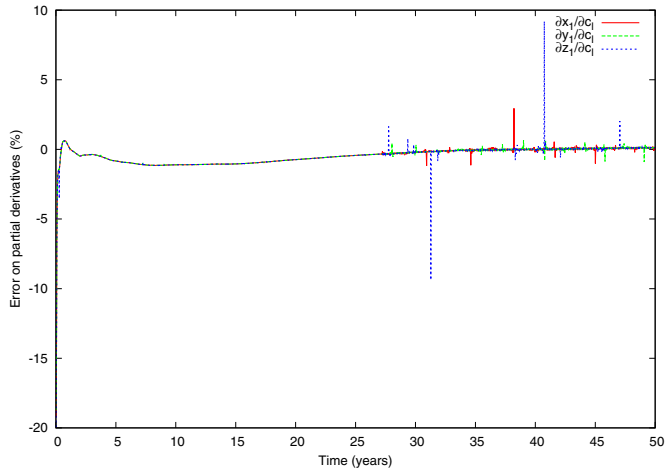

Figure 17. Variational equations test of Saturn's Q parameter from Mimas position.

(A color version of this figure is available in the online journal.)

subnebulae for all moons below Titan. However, it is fully compatible with a formation at the edge of Saturn's rings (Charnoz et al. 2011).

During all fitting procedures, we obtain an extra acceleration on Mimas' orbital longitude, related to a negative value of $da/dt = -(15.7 \pm 4.4) \times 10^{-15}$ AU day^{-1} (combination of all fit values). A possible source of error explaining such decay could be the proximity of Mimas to Saturn's halo. But if confirmed in the future, Mimas' orbital decay could have significant implications on Saturn's rings.

This work has been supported by EMERGENCE-UPMC grant (contract number: EME0911), FP7 program Europlanet-RI, EC grant (228319), and PNP (CNRS/INSU). The authors are indebted to all participants of the French Encelade WG and to Chloé Michaut. V.L. thanks Nick Cooper, Carl Murray, Michael Efroimsky, Alain Vienne, and Laurène Beauvalet for fruitful discussions.

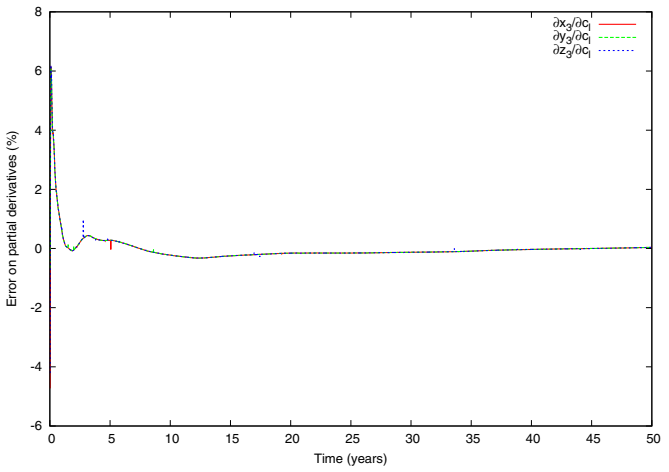

Figure 18. Variational equations test of Saturn's Q parameter from Tethys position.

(A color version of this figure is available in the online journal.)

APPENDIX

A.1. Testing Our Numerical Model

It is not possible to show the very large amount of tests that have been performed over years when developing the NOE code. Nevertheless, in the following section we provide several tests that can be considered as fundamental to our study.

Unless explicitly mentioned, the tested model here introduces the Enceladus equilibrium scenario with constant Q.

A.1.1. Numerical Precision

To test the numerical precision of our integrations of the equations of motion, we performed backward and forward integrations (see also the conservation of energy test). Figure 4 shows the difference, for each moon, between backward and forward integration expressed as Euclidian distance in km, over one century. These variations are all below 400 m. Since our integrations have been performed over no longer than 64 years (we recall that our fit epoch is 1950, and we cover the period 1886–2009), we can conclude that the numerical precision of the satellite positions in our study is a few hundreds of meters.

A.1.2. Conservation of Energy

Checking the conservation of energy is quite important for two reasons:

1. It provides another way to quantify numerical error (here the numerical accuracy).
2. More importantly, it checks the validity of the force model.

Nevertheless, energy is not always conserved for "any" force model (nonconservative forces, use of planetary ephemerides, introduction of forced precession, and spin–orbit coupling). In the following test (see Figure 5), we did not introduce (1) da/dt "force," (2) tidal dissipation, and (3) Saturn's precession. Moreover, solar and Saturnian motions have been integrated explicitly (no use of planetary ephemerides) and the rotation of the moons has been frozen.

As one can see in Figure 5, energy is conserved up to 13 digits (use of double precision) over 100 years, in our model.

A.1.3. Testing the Tidal Model

Since conservation of energy cannot be used to check the validity of our tidal model, we have used analytical expression

Table 6
Testing the Tidal Model (Tides in the Satellites/Two-body Problem)

Moon	Δa (km)	Δe
Mimas	−5.402801100992870E−002	−8.537669664267916E−006
Enceladus	−1.587689542119058E−003	−6.236475859717691E−007
Tethys	−1.229629000688473E−004	−2.139456833055286E−007
Dione	−8.724264672974581E−005	−6.140003928510260E−008
Rhea	−1.158774729219763E−005	−9.617269239444934E−009
Titan	−5.787519520775916E−004	−8.114568451206283E−009

of da/dt and de/dt to check the code. In particular, we recall that we have (as a first approximation) for the tides raised in the primary (Kaula 1964)

$$\frac{da}{dt} = \frac{3k_2 mnR^5}{QMa^4}\left(1+\frac{51}{4}e^2\right)$$
$$\frac{de}{dt} = \frac{57k_2 mn}{8QM}\left(\frac{R}{a}\right)^5 e \quad \text{(A1)}$$

and for the tides raised in the 1:1 spin–orbit satellite (Peale & Cassen 1978)

$$\frac{da}{dt} = -\frac{21k_2^s MnR_s^5}{Q^s ma^4}e^2$$
$$\frac{de}{dt} = -\frac{21k_2^s Mn}{2Q^s m}\left(\frac{R_s}{a}\right)^5 e \quad \text{(A2)}$$

To make the comparison straightforward, we first considered a two-body problem for each moon. However, integrating the Saturnian system by modeling only two-body interactions requires considering a different eccentricity when using Equations (A1) and (A2). In particular, we have found that using our nominal solution as initial conditions, the eccentricity of each moon was changed to 0.017011, 0.00534, 0.000976, 0.00188, 0.00114, and 0.02895 for Mimas to Titan, respectively.

Tides in the Planet (Two-body Problem). Over 100 years, variations on a are expected to be 8.37, 6.08, 10.722, 4.889, 1.641, 0.952 m for, respectively, S1, ..., S8 (Mimas, ..., Titan). Similarly, variations on e are expected to be 1.81×10^{-9}, 3.24×10^{-10}, 8.46×10^{-11}, 5.78×10^{-11}, 8.42×10^{-12}, and 5.30×10^{-11}.

Comparing such estimations with our numerical simulation offers a good agreement (see Figures 6 and 7; numerical table is available on request).

Tides in the Satellites (Two-body Problem). Over 100 years and assuming arbitrarily $k_2{}^s/Q^s = 10^{-2}$ for all moons, variations on a are expected to be −54.607, −1.597, −0.124, −0.087, −0.012, −0.544 m for, respectively, S1, ..., S8 (Mimas, ..., Titan). Similarly, variations on e are expected to be -8.66×10^{-6}, -6.28×10^{-7}, -2.15×10^{-7}, -6.15×10^{-8}, -9.61×10^{-9}, and -7.68×10^{-9}.

Our numerical simulation offers a good match with analytical formulation (see Figures 8 and 9 and Table 6). In particular, the use of a quite simplified force model greatly decreases numerical errors during integration, making the comparison possible (up to two digits at least, which may be the accuracy of the analytical formulation we consider).

Tides in the Planet (Full Model). One can try checking the tidal model with the full model considered in this work, even though perturbations will make the comparison with an analytical formulation more difficult. In particular, the expected drift on a and e may be masked by large short-period oscillations. Nevertheless, changes on a can still be checked by looking at the associated acceleration in longitude. Expected variations over 100 years in a from Equation (A1) are 8.38, 6.08, 10.72, 4.89, 1.64, and 0.95 m for Mimas to Titan, respectively. This translates to 1522, 761, 975, 306, 62, and 10 km in the mean longitudes.

In the simulations below, Tethys and Dione have been removed from the model to avoid resonances (which would make the analytic formulation of Equation (A1) invalid).

We obtain clearly a pretty good agreement (see Figures 10 and 11). A similar agreement can be found with the satellite case (full model).

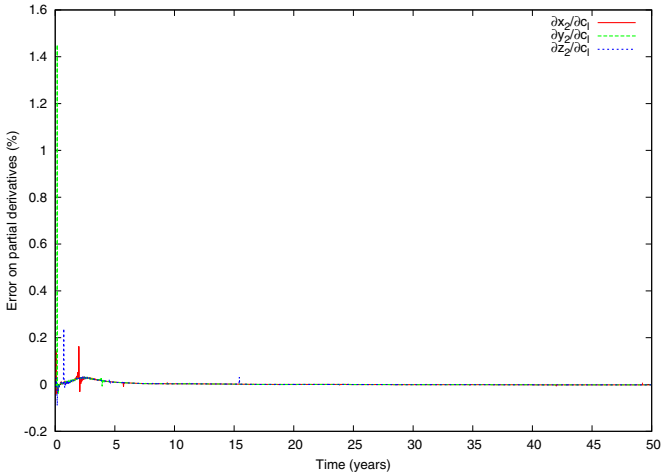

Figure 19. Variational equations test of Enceladus' Q parameter from Enceladus position.
(A color version of this figure is available in the online journal.)

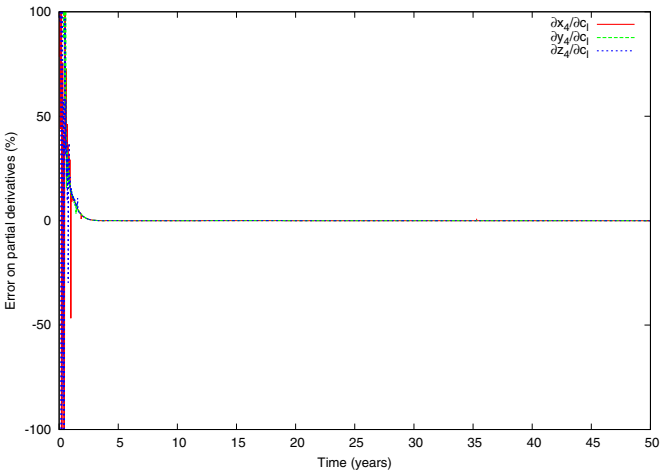

Figure 20. Variational equations test of Enceladus' Q parameter from Dione position.
(A color version of this figure is available in the online journal.)

A.1.4. Testing da/dt Acceleration

As for the tidal model, the "da/dt" force cannot be tested by the conservation of energy. Using Gauss' equations, we recall that we have introduced a force on Mimas that affects only its semi-major axis by a constant drift da/dt. Checking the validity of this force can be done easily by checking Mimas' semi-major axis variations after integration.

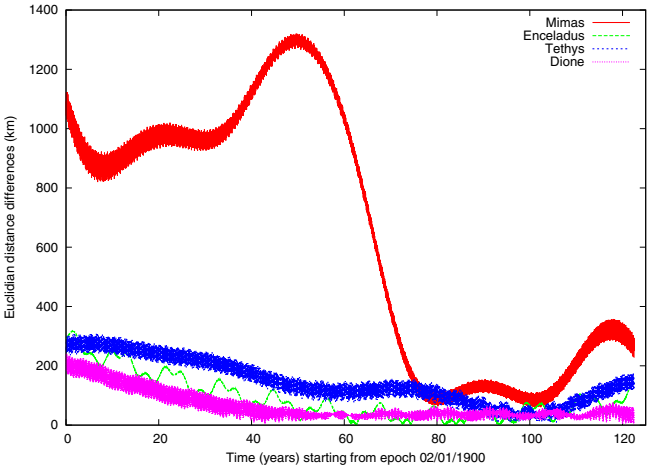

Figure 21. Position differences between JPL-SPICE sat317 ephemeris and the present work.

(A color version of this figure is available in the online journal.)

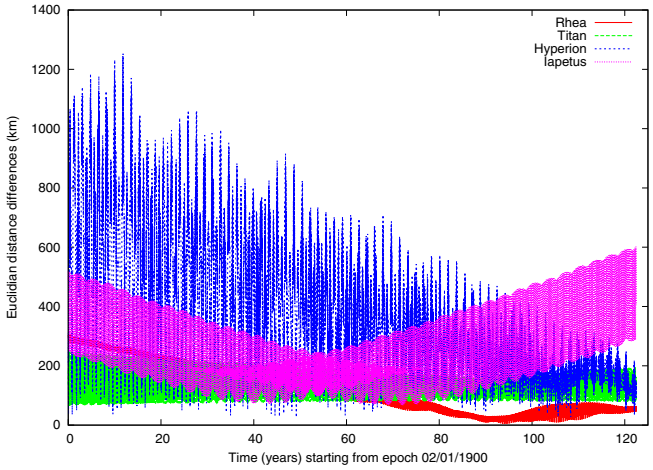

Figure 22. Position differences between JPL-SPICE sat317 ephemeris and the present work.

(A color version of this figure is available in the online journal.)

Here we consider the difference between two numerical simulations, with/without Mimas' da/dt (Mimas' semi-major axis input) equal to -16.9×10^{-15} AU day^{-1}.

Two-body Problem. We provide below such a test (Figure 12), assuming a two-body problem with only Saturn and Mimas. Clearly, the force acting on Mimas (input) and its expected effect on Mimas' semi-major axis (output) are in full agreement.

The other elements are not affected by the da/dt force, in the limit of accuracy of our integration.

Full Model. As for tidal effects, one may expect the comparison between input/output to be more difficult using the full model (Enceladus equilibrium scenario and constant Saturn's Q). Nevertheless, we can still use the mean longitude drift for the test and have a pretty good agreement with the two figures (Figures 13 and 14; Tethys has been removed from the simulation to avoid the Mimas–Tethys resonance). In particular, $da/dt = -16.9 \times 10^{-15}$ AU day^{-1} translates to 16,776 km in Mimas' mean longitude after 100 years. Figures 13 and 14 show the variations in semi-major axis and in positions (which corresponds essentially to the mean longitude variations).

A.1.5. Testing the Variational Equations

Partial derivatives of the moon state vectors as functions of initial conditions and physical parameters are computed by solving the so-called variational equations (see Equation (4)). Having accurate partial derivatives is a fundamental requirement when fitting a dynamical model to astrometric data. Solutions of the variational equations are routinely tested in our code. To check the accuracy of such computations, we compared our numerical solutions with their approximations using the centered difference method (i.e., $f'(x) \simeq [f(x+h) - f(x-h)]/2h$).

It is not possible to provide here the tests of all partial derivatives. Hence, we will restrict the number of figures by showing the computation of partial derivatives related to da/dt (Figures 15 and 16), Saturn's Q (Figures 17 and 18), and Enceladus' Q (denoted hereafter by Q^{s2}; Figures 19 and 20), only. Any other plots are available on request.

We recall that c_l denotes an unspecified parameter of the model that shall be fitted. For more details on the method used, we refer to Lainey et al. (2004).

Plots for $c_l = da/dt$ on Mimas position are shown in Figures 15 and 16.

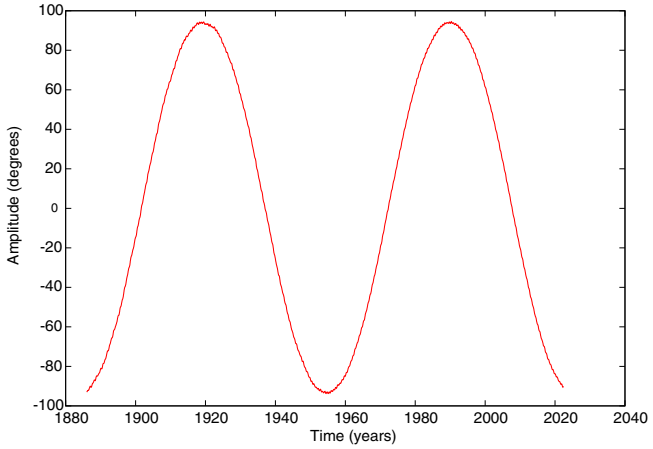

Figure 23. Mimas–Tethys resonant angle variation obtained with our model.

(A color version of this figure is available in the online journal.)

As can be seen in Figures 15 and 16, numerical computation of $\partial \boldsymbol{r}/\partial c_l$, where $\boldsymbol{r} = \boldsymbol{r}_1$ and $c_l = da/dt$, is in agreement with its approximation derived from the center difference method. The scattering behavior evident in Figure 15 is usual and corresponds to a nonlinear configuration occurring when the satellite reaches its maximum value along one Cartesian axis. As shown in Figure 16, these configurations occur when the distance differences (on the considered axis) are pretty small. Hence, this does not affect the fitting procedure. See also Lainey et al. (2004) for more details.

Plots for $c_l = Q$ on Mimas position and Tethys position are shown in Figures 17 and 18, respectively.

As can be seen in Figures 17 and 18, numerical computation of $\partial \boldsymbol{r}/\partial c_l$, where $\boldsymbol{r} = \boldsymbol{r}_1$ or $\boldsymbol{r} = \boldsymbol{r}_3$ and $c_l = Q$, is in agreement with its approximation derived from the center difference method.

Plots for $c_l = Q^{s2}$ on Enceladus position and Dione position are shown in Figures 19 and 20, respectively.

As can be seen in Figures 19 and 20, numerical computation of $\partial \boldsymbol{r}/\partial c_l$, where $\boldsymbol{r} = \boldsymbol{r}_2$ or $\boldsymbol{r} = \boldsymbol{r}_4$ and $c_l = Q^{s2}$, is in agreement with its approximation derived from the center difference method.

A.2. SPICE Kernel NOE-6-2011-MAIN.bsp

We have derived ephemerides of the eight main Saturnian moons for the Enceladus equilibrium and constant Q scenario. Our ephemerides are available as a SPICE kernel on the

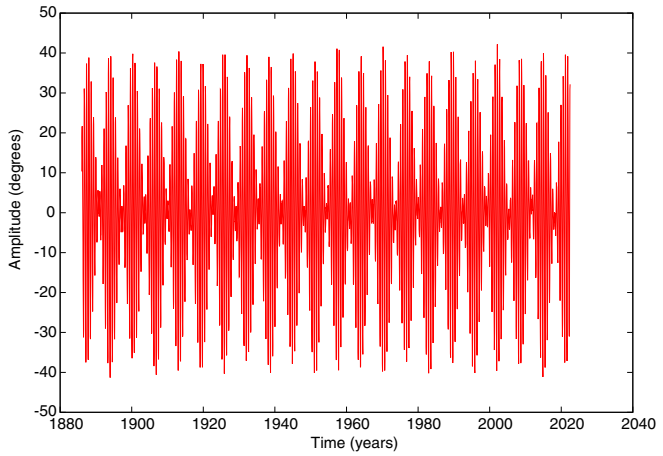

Figure 24. Enceladus–Dione resonant angle variation obtained with our model. (A color version of this figure is available in the online journal.)

FTP server of IMCCE: ftp://ftp.imcce.fr/pub/ephem/satel/NOE/SATURNE/.

Figures 21 and 22 show the Euclidian distance differences between our ephemerides and the JPL ones (kernel: sat317.bsp). Differences in the interval [1980, 2011] are between a few tens of km to less than 200 km, except for Hyperion and Iapetus, whose dynamics are less well constrained by the astrometric observations we used.

Since we have fitted a large da/dt term for Mimas, while JPL probably did not, one could expect large differences in Mimas' position. But as one can see, the large differences arise only before the 1970s. This suggests that it is the use of a large time span that makes possible the derivation of da/dt.

A.3. Resonances

While analytical developments require introducing explicitly orbital resonances, the latter are a simple consequence of initial conditions with numerical models. Figures 23 and 24 show the evolution of the resonant arguments associated with the Mimas–Tethys and Enceladus–Dione resonances, respectively.

REFERENCES

Abbot, R. I., Mulholland, J. D., & Shelus, P. J. 1975, AJ, 80, 723
Aitken, R. G. 1905, Lick Obs. Bul. No. 94
Aitken, R. G. 1909, Lick Obs. Bul. No. 172
Alden, H. L., & O'Connell, W. C. 1928, AJ, 38, 53
Alden, H. L. 1929, AJ, 40, 88
Archinal, B. A., A'Hearn, M. F., Bowell, E., et al. 2011, Celest. Mech. Dyn. Astron., 109, 101
Arlot, J.-E., & Emelyanov, N. V. 2009, A&A, 503, 631
Barnard, E. E. 1910, AJ, 26, 79
Barnard, E. E. 1913, AJ, 28, 1
Barnard, E. E. 1915, AJ, 29, 33
Barnard, E. E. 1916, AJ, 30, 33
Barnard, E. E. 1918, AJ, 31, 49
Barnard, E. E. 1927, AJ, 37, 157
Buratti, B. J. 1984, Icarus, 59, 392
Charnoz, S., Crida, A., Castillo-Rogez, J. C., et al. 2011, Icarus, 216, 535
Davies, M. E., Abalakin, V. K., Bursa, M., et al. 1996, Celest. Mech. Dyn. Astron., 63, 127
Desmars, J., Arlot, S., Arlot, J.-E., Lainey, V., & Vienne, A. 2009a, A&A, 499, 321
Desmars, J., Vienne, A., & Arlot, J. E. 2009b, A&A, 493, 1183
Dourneau, G., Veillet, C., Dulou, M. R., & Le Campion, J. F. 1986, A&A, 160, 280
Emelyanov, N. V., & Gilbert, R. 2006, A&A, 453, 1141
Fortney, J. F., & William, B. H. 2003, Icarus, 164, 228
French, R. G., McGhee, C. A., Frey, M., et al. 2006, PASP, 118, 246
Gavrilov, S. V., & Zharkov, V. N. 1977, Icarus, 32, 443
Goldreich, P., & Soter, S. 1966, Icarus, 5, 375
Goodman, J., & Lackner, C. 2009, ApJ, 696, 2054
Guillot, T. 1999, Science, 286, 72
Harper, D., Beurle, K., Williams, I. P., et al. 1999, A&AS, 136, 257
Harper, D., Murray, C. D., Beurle, K., et al. 1997, A&AS, 121, 65
Howett, C. J. A., Spencer, J. R., Pearl, J., & Segura, M. 2011, J. Geophys. Res., 116, E03003
Iorio, L., & Lainey, V. 2005, Int. J. Mod. Phys. D, 14, 2039
Jacobson, R. A. 2007, The Orientation and Precession of the Pole of Saturn, American Astronomical Society, DDA Meeting 38, 13.06
Jacobson, R. A., Antreasian, P. G., Bordi, J. J., et al. 2006, AJ, 132, 2520
Kaula, W. M. 1964, Rev. Geophys. Space Phys., 2, 661
Kiseleva, T. P., & Kalinitchenko, O. A. 1998, Pulkovo, Glavnaia Astronomicheskaia Observatoriia, Izvestiia, 213, 122
Kiseleva, T. P., & Kalinitchenko, O. A. 2000, Pulkovo, Glavnaia Astronomicheskaia Observatoriia, Izvestiia, 214, 344
Kiseleva, T. P., Kiselev, A. A., Khrutskaya, E. V., & Kalinitchenko, O. A. 1996, Pulkovo, Glavnaia Astronomicheskaia Observatoriia, Izvestiia, 210, 76
Lainey, V. 2008, Planet. Space Sci., 56, 1766
Lainey, V., Arlot, J. E., Karatekin, Ö., & Van Hoolst, T. 2009, Nature, 459, 957
Lainey, V., Dehant, V., & Pätzold, M. 2007, A&A, 465, 1075
Lainey, V., Duriez, L., & Vienne, A. 2004, A&A, 420, 1171
Lissauer, J. J., & Cuzzi, J. N. 1982, AJ, 87, 1051
Meyer, J., & Wisdom, J. 2007, Icarus, 188, 535
Morales, M. A., Schwegler, E., Ceperley, D., et al. 2009, Proc. Natl Acad. Sci., 106, 1324
Morgan, H. R. 1900, Astron. Nachr., 154, 91
Nimmo, F., Spencer, J. R., Pappalardo, R. T., & Mullen, M. E. 2007, Nature, 447, 289
Ogilvie, G. I., & Lin, D. N. C. 2004, ApJ, 610, 477
O'Neill, C., & Nimmo, F. 2010, Nat. Geosci., 3, 88, doi:10.1038/NGEO731
Peale, S. J., & Cassen, P. 1978, Icarus, 36, 245
Peng, Q., Vienne, A., & Shen, K. X. 2002, A&A, 383, 296
Peng, Q., Vienne, A., Wu, X. P., Gan, L. L., & Desmars, J. 2008, AJ, 136, 2214
Pitman, K. M., Buratti, B. J., & Mosher, J. A. 2010, Icarus, 206, 537
Porco, C. C., Helfenstein, P., Thomas, P. C., et al. 2006, Science, 311, 1393
Qiao, R. C., Shen, K. X., Harper, D., & Liu, J. R. 2004, A&A, 422, 377
Qiao, R. C., Shen, K. X., Liu, J. R., & Harper, D. 1999, A&AS, 137, 1
Rieutord, M., & Valdettaro, L. 2010, J. Fluid Mech., 643, 363
Seitzer, P., & Ianna, P. A. 1980, AJ, 85, 1117
Seitzer, P., Ianna, P. A., & Levinson, F. 1979, AJ, 84, 877
Sinclair, A. T. 1974, MNRAS, 169, 591
Sinclair, A. T. 1977, MNRAS, 180, 447
Sinclair, A. T. 1983, IAU Colloq. 74, Dynamical Trapping and Evolution in the Solar System, ed. V. V. Markellos & Y. Kozai (Dordrecht: Reidel), 19
Spencer, J. R., Barr, A. C., Esposito, L. W., et al. 2009, in Saturn from Cassini-Huygens, ed. M. K. Dougherty, L. W. Esposito, & S. M. Krimigis (Berlin: Springer), 683
Stone, O. 1895, AJ, 15, 110
Stone, O. 1896, AJ, 16, 62
Stone, O. 1898a, Astron. Nachr., 146, 223
Stone, O. 1898b, AJ, 19, 118
Stone, R. C., & Harris, F. H. 2000, AJ, 119, 1985
Struve, H. 1898, Publ. Obs. Central Nicolas, 11, 2
Struve, G. 1933, Veroff. Berlin-Babelsberg 6, parts 2, 3 and 5
Taylor, D. B., & Sinclair, A. T. 1985, A&AS, 61, 221
Thuillot, W., Arlot, J.-E., Ruatti, C., et al. 2001, A&A, 371, 343
Tobie, G., Cadek, O., & Sotin, C. 2008, Icarus, 196, 642
Tolbin, S. B. 1991a, Scientific paper deposited in All-russian institute of scientific and technical information, 3077-B91, 1
Tolbin, S. B. 1991b, Scientific paper deposited in All-russian institute of scientific and technical information, 3078-B91, 1
USNO 1929, Publ. U.S. Naval Obs., 12, 2
USNO 1954, Publ. U.S. Naval Obs., 17, 2
Vass, G. 1997, Roman. Astron. J., 7, 45
Veiga, C. H., Vieira Martins, R., Vienne, A., Thuillot, W., & Arlot, J. E. 2003, A&A, 400, 1095
Veillet, C., & Dourneau, G. 1992, A&AS, 94, 291
Vienne, A., Thuillot, W., Veiga, C. H., Arlot, J. E., & Vieira Martins, R. 2001, A&A, 380, 727
Voronenko, V. I., Gorel, G. K., Gudkova, L. A., & Pozhalova, J. A. 1991, Scientific paper deposited in All-russian institute of scientific and technical information, 3167-B91, 1
Wu, Y. 2005, ApJ, 635, 688
Zahn, J.-P. 1966, Ann. Astrophys., 29, 489
Zahn, J.-P. 1989, A&A, 220, 112